A reversible mesoscopic model of diffusion in liquids: from giant fluctuations to Fick's law

Aleksandar Donev,[1, *] Thomas G. Fai,[1] and Eric Vanden-Eijnden[1, †]

[1]Courant Institute of Mathematical Sciences,
New York University, New York, NY 10012

We study diffusive mixing in the presence of thermal fluctuations under the assumption of large Schmidt number. In this regime we obtain a limiting equation that contains a diffusive stochastic drift term with diffusion coefficient obeying a Stokes-Einstein relation, in addition to the expected advection by a random velocity. The overdamped limit correctly reproduces both the enhanced diffusion in the ensemble-averaged mean and the long-range correlated giant fluctuations in individual realizations of the mixing process, and is amenable to efficient numerical solution. Through a combination of Eulerian and Lagrangian numerical methods we demonstrate that diffusion in liquids is not most fundamentally described by Fick's irreversible law; rather, diffusion is better modeled as reversible random advection by thermal velocity fluctuations. We find that the diffusion coefficient is effectively renormalized to a value that depends on the scale of observation. Our work reveals somewhat unexpected connections between flows at small scales, dominated by thermal fluctuations, and flows at large scales, dominated by turbulent fluctuations.

I. Introduction

Diffusion is one of the most ubiquitous transport processes. It is, arguably, the simplest dissipative mechanism. Fick's law of diffusion is "derived" in most elementary textbooks, and relates diffusive fluxes to the gradient of chemical potentials via a diffusion coefficient that is typically thought of as an independent material property. There are several well-known hints that diffusion in liquids is, in fact, a rather subtle process. A first hint is that the Stokes-Einstein (SE) prediction for the diffusion coefficient is in surprisingly reasonable agreement with measurements even in cases where it should not apply at all, such as molecular diffusion. The fact that the SE prediction involves the viscosity of the fluid, a seemingly independent transport property, hints at the connection between momentum transport and diffusion. A second hint is the fact that nonequilibrium diffusive mixing is known to be accompanied by "giant" long-range correlated thermal fluctuations [1–3]. The enhancement of large-scale (small wavenumber) concentration fluctuations during free diffusive mixing has been measured using light scattering and shadowgraphy techniques [2, 4–6].

In either gases, liquids or solids, one can, at least in principle, coarse-grain Hamiltonian dynamics for the atoms (at the classical level) to obtain a model of diffusive mass transport at hydrodynamic scales. The actual coarse-graining procedure is, however, greatly simplified by first coarse-graining the microscopic dynamics to a simpler stochastic description. In the case of gases, mass transport can be modeled effectively using kinetic theory with cross-sections obtained from the underlying molecular interactions. In solids, atoms remain trapped around the crystal lattice sites for long periods of time and infrequently hop from site to site, so that diffusive transport can be modeled effectively at the microscopic level as a Markov Chain with transition rates that can be obtained from the molecular interactions using transition state theory. In both of these cases the picture that emerges is that of independent Brownian walkers performing uncorrelated random walks in continuum (gases) or on a lattice (solids). By contrast, in liquids the physical picture is rather different and must account for hydrodynamic correlations among the diffusing particles. In a liquid, molecules become trapped (caged) over long periods of time, as they collide frequently with their neighbors. Therefore, momentum and energy are exchanged (diffuse) much faster than the molecules themselves can escape their cage. The main mechanism by which molecules diffuse is the motion of the whole cage when a large-scale velocity fluctuation (coordinated motion of parcels of fluid) moves a group of molecules and shifts and rearranges the cage.

It is now well-understood that diffusion in liquids is strongly affected by advection by thermal velocity fluctuations [7–10]. The fact that thermal fluctuations exhibit long-ranged correlations in nonequilibrium settings has long been appreciated in statistical mechanics and nonequilibrium thermodynamics circles [1, 3]. The overarching importance of nonequilibrium fluctuations to transport in fluids has not, however, been widely appreciated. The microgravity experiments described in Ref. [6] show fluctuations of the

order of a fraction of a percent at millimeter scales. These results are a striking demonstration that thermal fluctuations are important not just at microscopic and mesoscopic scales, but also at *macroscopic* scales. Theoretical studies and computer simulations have verified that the advection by the thermally fluctuating fluid velocity leads to an *enhancement* or *renormalization* of the diffusion coefficient that depends on the viscosity of the fluid, and, importantly, on the dimensionality and imposed boundary conditions (in particular, system size) [8–10]. At the mathematical level, the diffusion enhancement is closely-related to the eddy diffusivity that arises in turbulent flows as mass is advected by the chaotic fluid velocity [11].

When modeling molecular diffusion, most theories are based on some form of mode-mode coupling, which is essentially a perturbative analysis in the strength of the thermal fluctuations [7, 12], starting from linearized fluctuating hydrodynamics. When modeling diffusion of particles suspended in a (complex) fluid, it is typically assumed that the immersed particle is either very large, much more massive, or both, compared to the fluid molecules [13]. In this work, for the first time, we bypass these types of approximations and develop a fully nonlinear fluctuating hydrodynamic description of diffusion that applies not only to a dilute suspension of large particles suspended in a simple liquid but also to molecular (self) diffusion of tagged molecules.

Here we formulate a simple model for diffusion in the presence of thermal velocity fluctuations and use it to make a precise assessment of the contribution of fluctuations to diffusive transport. In our model the momentum exchange is modeled using a continuum fluctuating hydrodynamic formalism, and represents the background fluctuating momentum (velocity) bath with which the diffusing particles (tracers) interact. We demonstrate that this simple model mimics all of the crucial features of realistic liquids, while also being tractable analytically and numerically, and showing rich physical behavior. Along the way we will construct a multiscale numerical method that can efficiently handle the practically-relevant case of very large Schmidt number. In our model we assume that the diffusing particles follow, on average, the locally-averaged (thermally fluctuating) velocity of the fluid. We further assume the existence of a large separation of time scales between the fast dynamics of the velocity (vorticity) fluctuations and the diffusive dynamics, i.e., we assume that the Schmidt number Sc (ratio of the diffusion coefficients of momentum and mass) is very large. This is known to be true in most liquids due to the effective caging of molecules in densely-packed liquid microstructures. In the limit Sc $\to \infty$ we can eliminate the fluid velocity using adiabatic mode elimination [14, 15] and obtain explicit results without resulting to perturbation analysis, as have previous studies.

Through a mix of theoretical and numerical studies, in this paper we demonstrate that over a broad range of length scales diffusion is better described as a reversible stochastic process, rather than an irreversible deterministic process as in Fick's law. This has the consequence that the diffusion coefficient (effective dissipation rate) is not a material constant, but rather depends on the scale of observation. Our work uncovers crucial distinctions between the Fickian diffusion of uncorrelated Brownian walkers and the non-Fickian collective diffusion of hydrodynamically-correlated tracers. We consider non-interacting particles, and make an important first step toward consistently including the effects of hydrodynamic correlations in fluctuating Dynamic Density Functional Theory (DDFT) [16–20] for suspensions of interacting colloids. Importantly, our work demonstrates that Fick's law for the average concentration is not affected by the presence of hydrodynamic interactions, and the non-local diffusion terms proposed in prior works [21, 22] do not actually appear. Some of our predictions could be used as a guide to design new Fluorescence Recovery After Photo-bleaching (FRAP) experiments to study the collective dynamics of tracer particles in liquids.

We begin by outlining our starting fluctuating hydrodynamics model for diffusion in the presence of thermal velocity fluctuations. These equations show extreme numerical stiffness at large Schmidt numbers and in Section II and Appendix A we obtain the limit of these equations as the Schmidt numbers becomes infinite. In Appendix II D we design Eulerian and Lagrangian numerical algorithms to solve the resulting advection-diffusion equation. In Section III we numerically and analytically study the difference between (dissipative and irreversible) classical Fickian diffusion and (conservative and reversible) diffusion by thermal velocity fluctuations, with particular focus on the appearance of giant fluctuations in the latter. In Section IV we discuss spatial coarse-graining of the limiting advection-diffusion equation, and summarize the emerging paradigm for how to accurately model diffusion in liquids over a broad range of scales. Finally, we offer some conclusions and a discussion of open challenges in Section V.

A. Advection-Diffusion Model

We consider the diffusion of passive tracer particles as they are advected by thermal velocity fluctuations. Examples include the diffusion of fluorescently-labeled macromolecules in solution, nano-colloidal particles in a nanofluid, and the self-diffusion of the molecules comprising a simple fluid. The hydrodynamic fluctuations of the fluid velocity $\boldsymbol{v}(\boldsymbol{r}, t)$ will be modeled via the linearized incompressible fluctuating

Navier-Stokes equation in d dimensions, $\boldsymbol{\nabla} \cdot \boldsymbol{v} = 0$, and

$$\rho \partial_t \boldsymbol{v} + \boldsymbol{\nabla} \pi = \eta \boldsymbol{\nabla}^2 \boldsymbol{v} + \sqrt{2\eta k_B T} \, \boldsymbol{\nabla} \cdot \boldsymbol{\mathcal{W}}, \tag{1}$$

where ρ is the fluid density, η the viscosity, and T the temperature, all assumed to be constant throughout the domain, and $\pi(\boldsymbol{r}, t)$ is the mechanical pressure. Here the stochastic momentum flux is modeled via a a white-noise symmetric tensor field $\boldsymbol{\mathcal{W}}(\boldsymbol{r}, t)$ with covariance chosen to obey a fluctuation-dissipation principle [3, 23],

$$\langle \mathcal{W}_{ij}(\boldsymbol{r}, t) \mathcal{W}_{kl}(\boldsymbol{r}', t') \rangle = (\delta_{ik}\delta_{jl} + \delta_{il}\delta_{jk}) \, \delta(t-t')\delta(\boldsymbol{r}-\boldsymbol{r}').$$

Note that because the noise is additive in (1) there is no difference between an Ito and a Stratonovich interpretation of the stochastic term.

The details of the coupling between the fluid and the passive tracer are complicated at the microscopic level [24] and some approximations are required to model the motion of the tracer. The principal effect of advection by the thermal velocity fluctuations can be captured by assuming that the position of a tracer $\boldsymbol{q}(t)$ follows a spatially smooth fluctuating velocity field $\boldsymbol{u}(\boldsymbol{r}, t)$,

$$d\boldsymbol{q}/dt = \boldsymbol{u}(\boldsymbol{q}, t) + \sqrt{2\chi_0} \, \boldsymbol{\mathcal{W}_q}(t), \tag{2}$$

where $\boldsymbol{\mathcal{W}_q}$ denotes a collection of d independent white-noise processes. Here χ_0 is a *bare* diffusion coefficient that can be thought of as representing a "random slip" relative to the local fluid velocity coming from the under-resolved microscopic dynamics, *uncorrelated* among distinct tracers. In what follows it will be crucial that $\boldsymbol{u}$ be divergence free, $\boldsymbol{\nabla} \cdot \boldsymbol{u} = 0$. In this work we assume that the velocity felt by the tracer,

$$\boldsymbol{u}(\boldsymbol{r}, t) = \int \boldsymbol{\sigma}(\boldsymbol{r}, \boldsymbol{r}') \, \boldsymbol{v}(\boldsymbol{r}', t) \, d\boldsymbol{r}' \equiv \boldsymbol{\sigma} \star \boldsymbol{v}, \tag{3}$$

is obtained by convolving [1] the fluid velocity with a smoothing kernel $\boldsymbol{\sigma}$ that filters out features at scales below a cutoff scale σ, the typical size of a tracer. For example, in the α-Navier-Stokes equations [25] the smoothing is chosen to be an inverse Helmholtz operator, $\boldsymbol{v} = \boldsymbol{u} - \sigma^2 \boldsymbol{\nabla}^2 \boldsymbol{u}$, with boundary conditions chosen such that $\boldsymbol{u}$ is divergence free within the domain of interest [26]. With periodic boundary conditions, in Fourier space, the inverse Helmholtz operator filter is $\hat{\boldsymbol{\sigma}}_{\boldsymbol{k}} = (1 + \sigma^2 k^2)^{-1} \boldsymbol{I}$.

It is important to point out that the smoothing or regularization of the fluctuating velocity field (3) is necessary. Otherwise, the diffusion coefficient of the tracer particle will diverge leading to an "ultraviolet catastrophe" familiar in renormalization theories. In the literature a phenomenological cutoff at large wavenumbers is imposed [7, 8, 12]. We implement this regularization here by applying a smooth filter to $\boldsymbol{v}$ to generate a velocity $\boldsymbol{u}$ with which we can advect tracers. Alternatively, one can filter the white-noise forcing in the velocity equation and replace $\boldsymbol{\mathcal{W}}$ by $\boldsymbol{\sigma} \star \boldsymbol{\mathcal{W}}$ in (1). In the end, as far as the passive tracers are concerned, the only thing that matters is the spatio-temporal spectrum of the advective velocity $\boldsymbol{u}(\boldsymbol{r}, t)$.

Let us assume that there are N tracers and define the concentration or density of tracers $c(\boldsymbol{r}, t) = \sum_{i=1}^{N} \delta(\boldsymbol{q}_i(t) - \boldsymbol{r})$. The Lagrangian description (2) of the dynamics of the individual tracers formally corresponds to an Eulerian description for the evolution of the concentration or number density of tracers $c(\boldsymbol{r}, t)$ via a fluctuating advection-diffusion Ito equation [19, 27],

$$\partial_t c = -\boldsymbol{u} \cdot \boldsymbol{\nabla} c + \chi_0 \boldsymbol{\nabla}^2 c + \boldsymbol{\nabla} \cdot \left(\sqrt{2\chi_0 c} \, \boldsymbol{\mathcal{W}}_c \right), \tag{4}$$

where $\boldsymbol{\mathcal{W}}_c(\boldsymbol{r}, t)$ denotes a white-noise vector field. It is important to point out that this equation is simply a formal rewriting of the equations of motion (2) for the N tracers and as such contains no new physical content. However, it can be argued that (4) also describes the dynamics of a spatially coarse-grained *smooth* concentration field when the density of tracers varies on a length scale much larger than the typical tracer distance [18, 28]. While a precise mathematical derivation of (4) from (2) is unavailable at present (but see [27] for a formal derivation) except in the case of no bare diffusion, $\chi_0 = 0$, we believe it is a very plausible fluctuating hydrodynamic model of self-diffusion or diffusion of dilute passive tracers in liquids.

As an illustration of the importance of thermal fluctuations in diffusive transport we use recently-developed

---

[1] In translationally-invariant systems (e.g., infinite or periodic systems) one can use standard convolution $\boldsymbol{\sigma}(\boldsymbol{r}, \boldsymbol{r}') \equiv \boldsymbol{\sigma}(\boldsymbol{r} - \boldsymbol{r}')$ and would typically take an isotropic kernel $\boldsymbol{\sigma}(\boldsymbol{r} - \boldsymbol{r}') = K_\sigma(\|\boldsymbol{r} - \boldsymbol{r}'\|)$, where $K_\sigma(r)$ is a symmetric "bell-shaped" function with support of length 2σ. When nontrivial boundary conditions are present (i.e., for confined systems), it is important to consider a more general filtering operation (mollification) that takes into account the boundary conditions. For certain types of boundary conditions the construction of $\boldsymbol{\sigma}(\boldsymbol{r}, \boldsymbol{r}')$ is nontrivial and ought be done on a case-by-case basis [25].
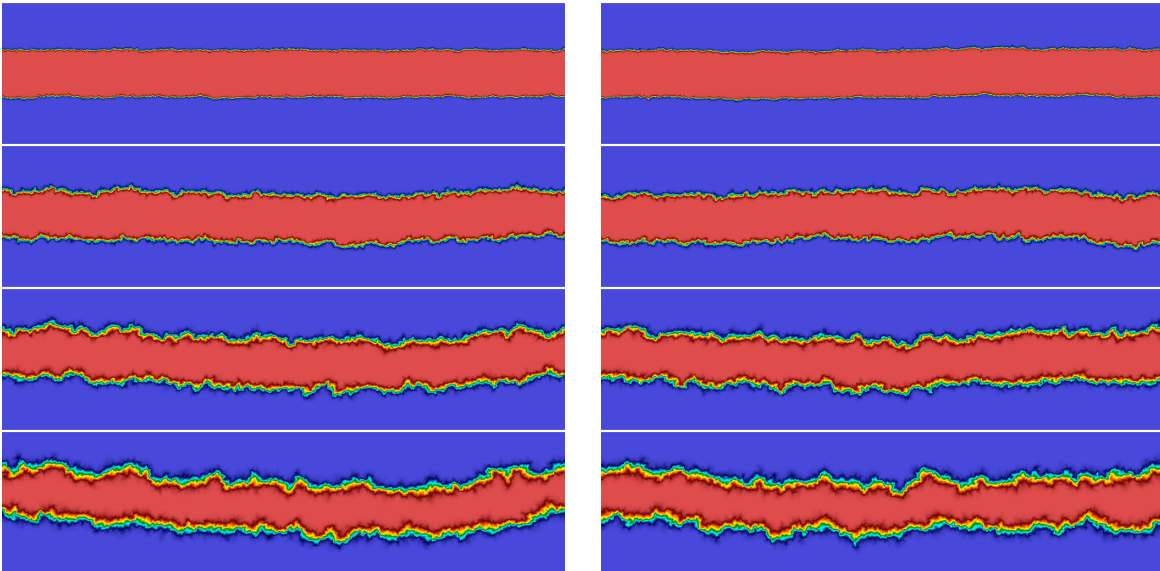
Figure 1: Snapshots of concentration showing the development of a *rough* diffusive interface between two miscible fluids, starting from concentration being unity in a horizontal (red) stripe occupying one third of the periodic domain, and zero elsewhere. We show four snapshots in time (evolving from top to bottom). The effective Schmidt number is Sc $\approx 1.5 \cdot 10^3$ and the bare diffusion is such that $\chi/\chi_0 \approx 5$. (*Left panel*) A single instance of the resolved dynamics (1,4). (*Right panel*) An independent instance of the limiting dynamics (5), or, equivalently, (9), obtained at a very small fraction ($10^{-3} \sim$ Sc^{-1}, see Section B 1) of the computational cost of the simulation shown in the left panel.

finite-volume numerical methods [29, 30] for solving (1,4) to model the diffusive mixing between two initially phase-separated fluids in two dimensions with periodic boundary conditions. In the left panel of Fig. 1 we show snapshots of the concentration field at several points in time. As seen in the figure, the interface between the fluids develops large-scale roughness (giant fluctuations) instead of remaining flat as in simple diffusion [6]. This roughening is accompanied by a slow spreading of the initially-sharp interface, similarly to what would be observed in deterministic diffusion. Molecular dynamics simulations have confirmed that fluctuating hydrodynamics accurately models the diffusive mixing process down to essentially molecular scales [31].

II.   The Limit of Large Schmidt Number

In liquids, diffusion of mass is much slower than diffusion of momentum, i.e., the Schmidt number is very large. More precisely, there is a large separation of time scales between the fast dynamics of the velocity fluctuations and the slow evolution of the concentration. This separation of time scales, to be verified *a posteriori*, can be used to perform a formal adiabatic mode-elimination procedure of the fast velocity degrees of freedom [15, 32–34] in (1,4). The mode-elimination procedure, which is detailed in Appendix A, gives a *limiting* stochastic advection-diffusion equation for the overdamped dynamics of the concentration,

$$\partial_t c = -\boldsymbol{w} \odot \boldsymbol{\nabla} c + \chi_0 \boldsymbol{\nabla}^2 c + \boldsymbol{\nabla} \cdot \left(\sqrt{2\chi_0 c} \, \boldsymbol{\mathcal{W}}_c \right), \tag{5}$$

where $\odot$ denotes a Stratonovich dot product, and the advection velocity $\boldsymbol{w}(\boldsymbol{r}, t)$ is white in time, with covariance proportional to a Green-Kubo integral of the velocity auto-correlation function,

$$\langle \boldsymbol{w}(\boldsymbol{r}, t) \otimes \boldsymbol{w}(\boldsymbol{r}', t') \rangle = \boldsymbol{\mathcal{R}}(\boldsymbol{r}, \boldsymbol{r}') \, \delta(t - t'), \tag{6}$$

$$\boldsymbol{\mathcal{R}}(\boldsymbol{r}, \boldsymbol{r}') = 2 \int_0^\infty \langle \boldsymbol{u}(\boldsymbol{r}, t) \otimes \boldsymbol{u}(\boldsymbol{r}', t + t') \rangle dt'. \tag{7}$$

The term $\boldsymbol{w} \odot \boldsymbol{\nabla} c$ is reminiscent of the random advection in the Kraichnan model of turbulent transport of a passive tracer [35, 36] (see section 4.1 in [11]).

To be more precise, let us perform a spectral decomposition of the covariance $\boldsymbol{\mathcal{R}}$ in some (infinite dimensional) set of (non-normalized) eigenfunctions $\boldsymbol{\phi}_k$,

$$\boldsymbol{\mathcal{R}}(\boldsymbol{r}, \boldsymbol{r}') = \sum_k \boldsymbol{\phi}_k(\boldsymbol{r}) \otimes \boldsymbol{\phi}_k(\boldsymbol{r}'). \tag{8}$$

The notation $\boldsymbol{w} \odot \boldsymbol{\nabla} c$ is short-hand for $\sum_k (\boldsymbol{\phi}_k \cdot \boldsymbol{\nabla} c) \circ d\mathcal{B}_k/dt$, where $\mathcal{B}_k(t)$ are independent Brownian motions (Wiener processes). In our numerical simulations, we use the Stratonovich form of the equations and apply an Euler-Heun (midpoint predictor-corrector) temporal integrator to (5).

For calculating ensemble averages, the Ito form of the equation is more useful. In the Ito interpretation, as derived in Appendix A, an unusual "thermal" or "Ito" drift appears in the limiting equation and takes the form of an *enhanced* diffusion,

$$\partial_t c = -\boldsymbol{w} \cdot \boldsymbol{\nabla} c + \boldsymbol{\nabla} \cdot [\boldsymbol{\chi}(\boldsymbol{r}) \boldsymbol{\nabla} c] + \chi_0 \boldsymbol{\nabla}^2 c + \boldsymbol{\nabla} \cdot \left(\sqrt{2\chi_0 c} \, \boldsymbol{\mathcal{W}}_c \right) \tag{9}$$

where the enhancement of the diffusion coefficient is given by the integral of the velocity autocorrelation function,

$$\boldsymbol{\chi}(\boldsymbol{r}) = \tfrac{1}{2} \boldsymbol{\mathcal{R}}(\boldsymbol{r}, \boldsymbol{r}) = \int_0^\infty \langle \boldsymbol{u}(\boldsymbol{r}, t) \otimes \boldsymbol{u}(\boldsymbol{r}, t+t') \rangle dt'. \tag{10}$$

Here we have made use of the fact that $\boldsymbol{\nabla} \cdot \boldsymbol{w} = 0$, and $\boldsymbol{w} \cdot \boldsymbol{\nabla} c$ is shorthand notation for $\sum_k (\boldsymbol{\phi}_k \cdot \boldsymbol{\nabla} c) \, d\mathcal{B}_k/dt$. The Ito equation (9) is the key result of the mode elimination procedure. The last two terms in this equation are deterministic diffusive terms, while the advective term $-\boldsymbol{w} \cdot \boldsymbol{\nabla} c$ is a (multiplicative) stochastic noise term that vanishes in the mean as a consequence of the Ito interpretation. That is, the ensemble average of the concentration obeys Fick's law,

$$\partial_t \langle c \rangle = \boldsymbol{\nabla} \cdot (\boldsymbol{\chi}_{\text{eff}} \boldsymbol{\nabla} \langle c \rangle) = \boldsymbol{\nabla} \cdot [(\chi_0 + \boldsymbol{\chi}) \boldsymbol{\nabla} \langle c \rangle], \tag{11}$$

which is a well-known result (c.f. (255) in Ref. [37]) that can be justified rigorously using stochastic homogenization theory [37]. In the absence of bare diffusion, $\chi_0 = 0$, the same equation (11) holds for *all* moments of c.

We note that (9) looks like an expected result but this is deceptive. While indeed the Green-Kubo expression for the diffusion coefficient of a tracer particle is well-known to be (10), what (9) is describing is the *collective* and not the *individual* diffusion of a tagged particle. The subtle difference between the two stems from the importance of the hydrodynamic correlations among the trajectories of the tracers. The "dissipative" term $\boldsymbol{\nabla} \cdot [\boldsymbol{\chi}(\boldsymbol{r}) \boldsymbol{\nabla} c]$ and the "fluctuating" term $-\boldsymbol{w} \cdot \boldsymbol{\nabla} c$ are signatures of the same physical process, advection by thermal velocity fluctuations. This is most clearly seen in the Stratonovich form (5) where there is only a single stochastic term $-\boldsymbol{w} \odot \boldsymbol{\nabla} c$ present. The stochastic advection term in (9) need to be retained to obtain the giant fluctuations seen in a *particular instance* (realization) of the diffusive mixing process. Including the dissipative term $\boldsymbol{\nabla} \cdot [\boldsymbol{\chi}(\boldsymbol{r}) \boldsymbol{\nabla} c]$ but omitting the random advection term $-\boldsymbol{w} \cdot \boldsymbol{\nabla} c$ violates fluctuation-dissipation balance and *cannot* be justified by simply arguing that the fluctuating term has mean zero. Just like the stochastic noise term $\boldsymbol{\nabla} \cdot \left(\sqrt{2\chi_0 c} \, \boldsymbol{\mathcal{W}}_c \right)$ corresponds to (i.e., is in fluctuation-dissipation balance with) the dissipative term $\chi_0 \boldsymbol{\nabla}^2 c$ for a collection of uncorrelated random walkers, the stochastic noise term $-\boldsymbol{w} \cdot \boldsymbol{\nabla} c$ corresponds to the Fickian term $\boldsymbol{\nabla} \cdot [\boldsymbol{\chi}(\boldsymbol{r}) \boldsymbol{\nabla} c]$ for a collection of hydrodynamically correlated tracers. While the dissipation in both cases looks like simple diffusion, the important distinction between the two types of microscopic dynamics is made clear in the stochastic forcing term.

A. The Stokes-Einstein Relation

In the overdamped limit, the details of the evolution of the fluid velocity do not matter, so long as there exists a unique time-reversible equilibrium dynamics over which the average in (7) is taken. If one assumes the linearized fluctuating Navier-Stokes equation (1) holds, then it is not hard to show that

$$\int_0^\infty \langle \boldsymbol{v}(\boldsymbol{r}, t) \otimes \boldsymbol{v}(\boldsymbol{r}', t+t') \rangle dt' = \frac{k_B T}{\eta} \boldsymbol{G}(\boldsymbol{r}, \boldsymbol{r}'), \tag{12}$$

where $\boldsymbol{G}$ is the Green's function (Oseen tensor) for the steady Stokes equation [2] with unit viscosity, $\boldsymbol{v} = \boldsymbol{G} \star \boldsymbol{f}$ if $\boldsymbol{\nabla} \pi = \boldsymbol{\nabla}^2 \boldsymbol{v} + \boldsymbol{f}$ subject to $\boldsymbol{\nabla} \cdot \boldsymbol{v} = 0$ and appropriate boundary conditions. A sample of the Brownian increment $\sum_k \boldsymbol{\phi}_k d\mathcal{B}_k$ can be obtained by solving a steady Stokes problem with a suitable random forcing (fluctuating stress), and then convolving the velocity with the filter $\boldsymbol{\sigma}$.

The diffusion enhancement (10) can be obtained explicitly from (12) as

$$\boldsymbol{\chi}(\boldsymbol{r}) = \frac{k_B T}{\eta} \int \boldsymbol{\sigma}(\boldsymbol{r}, \boldsymbol{r}') \boldsymbol{G}(\boldsymbol{r}', \boldsymbol{r}'') \boldsymbol{\sigma}^T(\boldsymbol{r}, \boldsymbol{r}'') \, d\boldsymbol{r}' d\boldsymbol{r}''. \tag{13}$$

---

[2] For unbounded three-dimensional systems the Oseen tensor is $\boldsymbol{G}(\boldsymbol{r}', \boldsymbol{r}'') = (8\pi r)^{-1} \left(\boldsymbol{I} + r^{-2} \boldsymbol{r} \otimes \boldsymbol{r} \right)$, where $\boldsymbol{r} = \boldsymbol{r}' - \boldsymbol{r}''$.

The relation (13) is nothing more than the Stokes-Einstein (SE) relation $\boldsymbol{\chi}(\boldsymbol{q}) = k_B T \boldsymbol{\mu}(\boldsymbol{q})$, where $\boldsymbol{\mu}$ is the *deterministic* mobility of one of the tracers, defined via the relation $\boldsymbol{u} = \boldsymbol{\mu} \boldsymbol{F}$, where $\boldsymbol{F}$ is a constant force applied on a tracer at position $\boldsymbol{q}$ and $\boldsymbol{u}$ is the resulting velocity of the tracer [38]. Namely, the applied force can easily be included in our model as an additional force density $\boldsymbol{f}(\boldsymbol{r}) = \boldsymbol{\sigma}^T(\boldsymbol{q}, \boldsymbol{r}) \boldsymbol{F}$ in the steady Stokes equation [38, 39], which directly leads to the SE relation (13). This shows that the diffusion enhancement $\boldsymbol{\chi}(\boldsymbol{r})$ is consistent with the SE relation, as expected, validating the model.

To get an intuitive understanding and an estimate of the diffusion enhancement $\boldsymbol{\chi}$ we consider an infinite isotropic system and introduce a cutoff for the fluctuations in the advective velocity $\boldsymbol{w}$ at *both* large and small scales. The large-scale cutoff corresponds to a finite extent of the system L, and the small-scale cutoff corresponds to the filtering at the molecular scale σ. According to (12), at intermediate scales the Fourier spectrum of $\boldsymbol{w}$ should match the Green's function for Stokes flow with unit density and viscosity, $\widehat{\boldsymbol{G}}_{\boldsymbol{k}} = k^{-2}(\boldsymbol{I} - k^{-2}\boldsymbol{k} \otimes \boldsymbol{k})$ for wavevector $\boldsymbol{k}$. As an example, we choose an isotropic filtering kernel $\boldsymbol{\sigma}(\boldsymbol{r}, \boldsymbol{r}') = \varsigma(\|\boldsymbol{r} - \boldsymbol{r}'\|) \boldsymbol{I}$ giving $\mathcal{R}(\boldsymbol{r}, \boldsymbol{r}') = \mathcal{R}(\|\boldsymbol{r} - \boldsymbol{r}'\|)$, such that the Fourier transform of (13), $\hat{\boldsymbol{\mathcal{R}}}_{\boldsymbol{k}} = 2(k_B T/\eta)|\hat{\varsigma}_{\boldsymbol{k}}|^2 \widehat{\boldsymbol{G}}_{\boldsymbol{k}}$, has the form

$$\hat{\boldsymbol{\mathcal{R}}}_{\boldsymbol{k}} = \frac{2k_B T}{\eta} \frac{k^2 L^4}{(1 + k^4 L^4)(1 + k^2 \sigma^2)} \left(\boldsymbol{I} - \frac{\boldsymbol{k} \otimes \boldsymbol{k}}{k^2} \right). \tag{14}$$

This particular form is chosen for convenience and not because of any particular physical importance; the important thing is that at intermediate $L^{-1} \ll k \ll \sigma^{-1}$ we have $\hat{\varsigma}_{\boldsymbol{k}} \approx 1$, that $|\hat{\varsigma}_{\boldsymbol{k}}| \ll 1$ for $k \ll L^{-1}$ and vanishes [3] at $\boldsymbol{k} = \boldsymbol{0}$, and that $\hat{\boldsymbol{\mathcal{R}}}_{\boldsymbol{k}}$ decays faster than k^{-d} for $k \gg \sigma^{-1}$. Converting (14) to real space gives an isotropic enhancement to the diffusion tensor $\boldsymbol{\chi} = \boldsymbol{\mathcal{R}}(0)/2 = (2\pi)^{-d} \int \left(\hat{\boldsymbol{\mathcal{R}}}_{\boldsymbol{k}}/2 \right) d\boldsymbol{k} = \chi \boldsymbol{I}$. Note that this Fourier integral is exactly the one that appears in the linearized steady-state (static) approximate renormalization theory [7, 12] when $\nu \gg \chi_0$ (c.f. Eq. (12) in [9]). This is expected since in the end all approaches lead to the familiar SE formula for the diffusion coefficient of an individual tracer (but recall the important distinction between the individual and collective diffusion). Our derivation shows that the SE relation can be seen as a formula for the eddy-diffusivity due to advection by a thermally-fluctuating random velocity field.

Performing the integral of (14) in spherical coordinates gives an asymptotic expansion in σ/L,

$$\chi = \frac{k_B T}{\eta} \begin{cases} (4\pi)^{-1} \ln \frac{L}{\sigma} & \text{if } d = 2 \\ (6\pi\sigma)^{-1} \left(1 - \frac{\sqrt{2}}{2} \frac{\sigma}{L} \right) & \text{if } d = 3. \end{cases} \tag{15}$$

Note that in three dimensions the coefficients $\sqrt{2}/2$ and the 6π in the denominator in (15) depend on the exact form of the spectrum $\hat{\chi}_{\boldsymbol{k}}$, but the coefficient of 4π in two dimensions does *not* depend on the details of the spectrum at small and large k. For an isotropic Gaussian filter $\boldsymbol{\sigma}$ with standard deviation σ, as employed in our Lagrangian numerical algorithm, for a periodic domain of length L the diffusion enhancement has a form similar to (15), $\chi = k_B T (4\pi\eta)^{-1} \ln[L/(\alpha\sigma)]$ in two dimensions, where we numerically estimate the coefficient $\alpha \approx 5.5$. When $L \gg \sigma$, in three dimensions (15) gives the Stokes-Einstein prediction $\chi \approx \chi_{SE} = k_B T/(6\pi\eta\sigma)$ for the diffusion coefficient of a slowly-diffusing no-slip rigid sphere of radius σ. In two dimensions, the effective diffusion coefficient grows logarithmically with system size, in agreement with the Einstein relation and the Stokes paradox for the mobility of a disk of radius σ. This system-size dependence of the effective diffusion coefficient was quantitatively verified using steady-state particle simulations in Refs. [9, 40].

It is important to note that (13) continues to hold in bounded domains also, and can be used to obtain expressions for the position-dependent tensor diffusion coefficient $\boldsymbol{\chi}(\boldsymbol{r})$ of a tracer particle in confined domains such as nano-channels [10, 41]. Similarly, (9) can describe the collective diffusion of many tracers through a nano-channel. In confined geometry, the Green's function $\boldsymbol{G}$ can be expressed as an infinite series $\boldsymbol{G}(\boldsymbol{r}, \boldsymbol{r}') = \sum_k \lambda_k^{-1} \boldsymbol{\varphi}_k(\boldsymbol{r}) \otimes \boldsymbol{\varphi}_k(\boldsymbol{r}')$, where $\boldsymbol{\varphi}_k$ are a set of orthonormal eigenfunctions of the Stokes problem (with the appropriate boundary conditions), and λ_k are the associated eigenvalues. Note that the eigenfunctions used to factorize the covariance of $\boldsymbol{w}$ in (8) can be written as $\boldsymbol{\phi}_k = \sqrt{\lambda_k} \boldsymbol{\sigma} \star \boldsymbol{\varphi}_k$ for the case when $\boldsymbol{v}$ follows the fluctuating Stokes equation.

Having obtained and analyzed the limiting dynamics, we are in a position to ascertain the validity of

---

[3] An alternative approach is to make the lower bound for integrals in Fourier space be $k = 2\pi/L$, mimicking a Fourier series for a cubic box of length L.

the initial assumption of large separation of time scales between concentration and momentum diffusion. Specifically, the limiting equations (5,9) [similarly, (16,17)] are good approximations to (4) [correspondingly, (2)] if the effective Schmidt number $Sc = \nu/\chi_{\text{eff}} = \nu/(\chi_0 + \chi) \gg 1$, where $\nu = \eta/\rho$ is the kinematic viscosity (momentum diffusion coefficient). This is indeed the case in practice for both simple liquids and especially for macromolecular solutions.

B.   Relation to Brownian Dynamics

In the Lagrangian description, the overdamped limit of (2) in the Stratonovich interpretation can be shown to be

$$d\boldsymbol{q} = \sum_k \boldsymbol{\phi}_k\left(\boldsymbol{q}\right) \circ d\mathcal{B}_k + \sqrt{2\chi_0}\, d\boldsymbol{\mathcal{B}_q}. \tag{16}$$

This derivation is not presented here but is rather standard and follows the procedure outlined in Appendix A, albeit greatly simplified by the finite-dimensional character of the limiting equation. The second stochastic term on the right hand side of (16) uses an independent Brownian motion $\boldsymbol{\mathcal{B}_q}(t)$ for each Brownian walker (tracer). The first stochastic forcing term uses a *single* realization of the random field $\sum_k \boldsymbol{\phi}_k \circ d\mathcal{B}_k$ for *all* of the walkers, and therefore induces correlations between the trajectories of the tracers. In the Ito interpretation the Lagrangian overdamped dynamics takes the form

$$d\boldsymbol{q} = \sum_k \boldsymbol{\phi}_k\left(\boldsymbol{q}\right) d\mathcal{B}_k + \left[\partial_{\boldsymbol{q}} \cdot \boldsymbol{\chi}\left(\boldsymbol{q}\right)\right] dt + \sqrt{2\chi_0}\, d\boldsymbol{\mathcal{B}_q}. \tag{17}$$

For translationally-invariant systems the thermal or stochasic drift term vanishes because $\boldsymbol{\chi}$ is independent of the position of tracer, $\partial_{\boldsymbol{q}} \cdot \boldsymbol{\chi} = \boldsymbol{0}$. In the more general case, it can be shown from (6) that $\partial_{\boldsymbol{q}} \cdot \boldsymbol{\chi}\left(\boldsymbol{q}\right) = \sum_k \boldsymbol{\phi}_k\left(\boldsymbol{q}\right) \cdot \boldsymbol{\nabla}\boldsymbol{\phi}_k\left(\boldsymbol{q}\right)$.

Our overdamped Lagrangian equations (17) are *equivalent* in form to the standard equations of Brownian Dynamics (BD), which are commonly used to model dynamics of colloidal particles or polymer chains in flow [42, 43]. In the absence of external forces, BD is typically presented as solving the Ito equations of motion for the (correlated) positions of the N tracers (Brownian walkers) $\boldsymbol{Q} = \{\boldsymbol{q}_1, \ldots, \boldsymbol{q}_N\}$,

$$d\boldsymbol{Q} = \left(2k_B T\, \boldsymbol{M}\right)^{\frac{1}{2}} d\boldsymbol{\mathcal{B}} + k_B T\left(\partial_{\boldsymbol{Q}} \cdot \boldsymbol{M}\right) dt + \sqrt{2\chi_0}\, d\boldsymbol{\mathcal{B}_Q}, \tag{18}$$

where $\boldsymbol{M}\left(\boldsymbol{Q}\right)$ is the *mobility* block matrix for the collection of particles [39]. Equation (18) is equivalent to (17) with the identification of the mobility tensor for a pair of particles i and j,

$$\boldsymbol{M}_{ij}\left(\boldsymbol{q}_i, \boldsymbol{q}_j\right) = \frac{1}{2k_B T} \sum_k \boldsymbol{\phi}_k\left(\boldsymbol{q}_i\right) \boldsymbol{\phi}_k\left(\boldsymbol{q}_j\right) = \frac{\boldsymbol{\mathcal{R}}\left(\boldsymbol{q}_i, \boldsymbol{q}_j\right)}{2k_B T}.$$

If we write this explicitly for Stokes flow using (12) we get (see, for example, Eq. (3.25) in Ref. [44]),

$$\boldsymbol{M}_{ij}\left(\boldsymbol{q}_i, \boldsymbol{q}_j\right) = \eta^{-1} \int \boldsymbol{\sigma}\left(\boldsymbol{q}_i, \boldsymbol{r}'\right) \boldsymbol{G}\left(\boldsymbol{r}', \boldsymbol{r}''\right) \boldsymbol{\sigma}^T\left(\boldsymbol{q}_j, \boldsymbol{r}''\right) d\boldsymbol{r}' d\boldsymbol{r}''. \tag{19}$$

When the particles are far apart, $\|\boldsymbol{q}_i - \boldsymbol{q}_j\| \gg \sigma$, the mobility is well-approximated by the Oseen tensor, $\boldsymbol{M}_{ij}\left(\boldsymbol{q}_i, \boldsymbol{q}_j\right) \approx \eta^{-1}\boldsymbol{G}\left(\boldsymbol{q}_i, \boldsymbol{q}_j\right)$. At short distances the divergence of the Oseen tensor is mollified by the filter, and (19) gives a pairwise mobility very similar to the Rotne-Prager-Yamakawa (RPY) mobility used in BD simulations [45]. In future work [27] we will show that one can start from the overdamped Lagrangian equations (17), or equivalently, (18), and follow an argument similar to the one of Dean [19], which omits hydrodynamic correlations, to construct an overdamped Eulerian equation for the empirical concentration $c\left(\boldsymbol{r}, t\right) = \sum_{i=1}^{N} \delta\left(\boldsymbol{q}_i\left(t\right) - \boldsymbol{r}\right)$. Such a calculation leads to the same equation (9) as we obtained here by rather different means, and demonstrates that hydrodynamic interactions do not modify Fick's law (11) for the mean concentration. It has been suggested that non-local diffusion terms appear when hydrodynamics is accounted for [21, 46]; however, this prior work fails to notice that for the RPY mobility these terms actually disappear as a direct consequence of the incompressibility of the fluid flow.

In principle, traditional BD can be used to study the Lagrangian tracer dynamics numerically. This has in fact been done by some authors in turbulence to study multi-particle correlations of a *few* passive tracers [47]. A key difference is that in traditional BD the stochastic terms are generated by applying some form of square root of the mobility $\boldsymbol{M}\left(\boldsymbol{Q}\right)$, which can be expensive for many tracers unless specialized fast multipole techniques are employed [42, 48]. By contrast, in the equivalent formulation (17) the stochastic forcing is generated by evaluating a random velocity field at the positions of the tracers. This formulation leads to a simple Lagrangian algorithm that is *linear* in the number of tracers N, as we discuss in Section II D.

C. Relation to mode-mode coupling and renormalization theories

The fact that thermal velocity fluctuations enhance diffusion is well known and there are several mode-mode coupling calculations that eventually lead to a similar result to our Stokes-Einstein formula (13). A key difference between our approach and other derivations is the fact that our calculation replaced typical *uncontrolled* approximations by a precise set of initial assumptions, and leads to a *rigorous* closed-form fluctuating advection-diffusion equation (17) for the concentration. In traditional perturbative renormalization approaches [7–9, 12, 13], one starts from equations that already have diffusion (dissipation) in them, and then considers what perturbation the fluctuations make. In this sense, Fick's linear law is the zeroth order approximation, and the first order perturbation is *linearized* fluctuating hydrodynamics. At the next order the fluctuations are found to give rise to Fick's law with a renormalized diffusion obeying a Stokes-Einstein relation [8]. This leads to a circular argument in which the physical phenomenon included in the lowest order approximation is the result of higher-order approximations, and an infinite sequence of renormalization steps is required to make the model self-consistent. Our work shows that the problem is quite simply and straightforwardly solved by starting with a *non-linear model* that then self-consistently gives rise to "renormalized" diffusion, instead of starting with a model that has diffusion put in as input and then linearizing.

While the physical difference between two and three dimensional fluctuations has been long appreciated in the literature, we believe our approach is not only simpler, but also more effective and more illuminating than mode-mode coupling analysis. There has been some confusion in the literature about the applicability of hydrodynamics to two dimensional systems, and statements to the effect that Stokes-Einstein does not apply in two dimensions have been made [49]. We showed that for finite systems nonlinear fluctuating hydrodynamics does lead to Stokes-Einstein relation for the diffusion coefficient in Fick's law (11) for the ensemble *mean*. One of the reasons we are able to easily obtain results is our use of the separation of time scales. We note, however, that the assumption of infinite Schmidt number, crucial to our approach, has to fail in *very* large two dimensional systems. Namely, large-scale (slow) velocity modes make a crucial contribution to diffusion, which itself occurs at faster time scales as the system grows due to the increasing diffusion coefficient. At finite Schmidt numbers the situation is much more complex and even mode-mode coupling theories run into problems [50]. The asymptotic behavior of the system of equations (1,4) in two dimensions in the infinite system size (thermodynamic) limit remains an interesting open question [38].

D. Multiscale Numerical Algorithms

Details of our multiscale numerical algorithms for solving the limiting Eulerian (5) and Lagrangian (16) equations are given in Appendix B; here we briefly summarize the key features.

We have developed finite-volume numerical methods to simulate the limiting dynamics (5), detailed in Section B 1. The spatial discretization of the advective term $\boldsymbol{w} \odot \boldsymbol{\nabla} c$ is identical to the one described in Ref. [29], and is constructed to ensure that advection is discretely non-dissipative. A pseudo-spectral steady-Stokes solver is used to generate a random advection velocity $\boldsymbol{w}$. The temporal integrator uses the implicit midpoint rule for the term $\chi_0 \boldsymbol{\nabla}^2 c$ [29], and the Euler-Heun method [4] for the term $\boldsymbol{w} \odot \boldsymbol{\nabla} c$. This approach is chosen because it ensures fluctuation-dissipation balance between the enhanced diffusion and the random advection. Note that in this numerical method the small-scale cutoff σ is related to the grid spacing employed in the finite-volume grid. The results of our numerical algorithm are compared to the results for the resolved dynamics (1,4) in Fig. 1. Visually the two figure panels are indistinguishable, and more detailed analysis has not found any statistically significant differences. It is, however, important to point out that the multiscale method employing the limiting dynamics can reach the same time scales in *much* less computational effort than the direct numerical simulation because it avoids the need to resolve the fast velocity fluctuations. Because it plays little role far from equilibrium and does not affect the giant fluctuations that are the focus of our study, we do not include the multiplicative noise term $\boldsymbol{\nabla} \cdot \left(\sqrt{2\chi_0 c} \, \boldsymbol{\mathcal{W}}_c \right)$ from the concentration equation in all of the Eulerian numerical simulations reported here.

We cannot study the case of no bare diffusion, $\chi_0 = 0$, using an *Eulerian* grid-based algorithm. Because advection creates finer and finer scales in the solution, truncation on a regular grid leads to a Gibbs phenomenon and ultimately numerical instability. We are, in fact, not aware of any Eulerian numerical method that could be used to reliably study the limiting case $\chi_0 = 0$ without introducing artificial

---

[4] The Euler-Heun method is a predictor-corrector algorithm that can be can be thought of as the Stratonovich equivalent of the Euler-Maruyama method for Ito stochastic differential equations.

dissipation. We have therefore developed a *Lagrangian* tracer algorithm to solve (16), detailed in Section B 2. In the Lagrangian algorithm, a realization of the advection velocity field $\boldsymbol{w}(\boldsymbol{r}, t)$ is sampled using a spectral steady Stokes solver, a convolution with a Gaussian function of standard deviation σ is used to filter the small scales, and a non-uniform FFT algorithm [51] is used to evaluate $\boldsymbol{w}(\boldsymbol{q}, t)$. This approach leads to a scheme in which the only truncation (discretization) error comes from the Euler-Heun temporal integrator.

The Lagrangian approach is particularly useful when the tracers model actual physical particles that can be tracked individually, for example, fluorescently-labeled molecules in a FRAP experiment. The Lagrangian tracing algorithm can also be used to solve (5,9) in the abscence of bare diffusion by employing the identity $c(\boldsymbol{q}(t), t) = c(\boldsymbol{q}(0), 0)$. Because the Lagrangian trajectories are time-reversible, one can obtain the concentration at a given position $\boldsymbol{r}$ by starting a tracer from $\boldsymbol{q}(0) = \boldsymbol{r}$, following its trajectory for a time t, and then evaluating the initial condition at the new position of the tracer, $c(\boldsymbol{q}(0), t) = c(\boldsymbol{q}(t), 0)$. The Lagrangian approach leads to a spatial discretization of (5) that is free of artificial dispersion or dissipation, with the main source of numerical error coming from the fact that a finite number of tracers is employed.

III. Is Diffusion in Liquids Irreversible?

The well-known fact that the measured diffusion coefficients in molecular liquids and macromolecular solutions closely match the Stokes-Einstein prediction hints that in realistic fluids diffusive transport is dominated by advection by the velocity fluctuations, $\chi \gg \chi_0$. This suggests that it is relevant to consider the case of no bare diffusion. If $\chi_0 = 0$, the evolution of the mean is dissipative since $\chi_{\text{eff}} = \chi > 0$. However, each realization follows a strictly reversible dynamics. It is not difficult to appreciate that an instance of a random process can behave very differently from the ensemble mean. For example, the average over many randomly dephasing oscillators will produce a decaying amplitude, even though each instance is non-decaying. It is therefore important to understand the difference in the behavior of the ensemble mean of the diffusive mixing process, described by (11), and the behavior of an individual realization, described by (5).
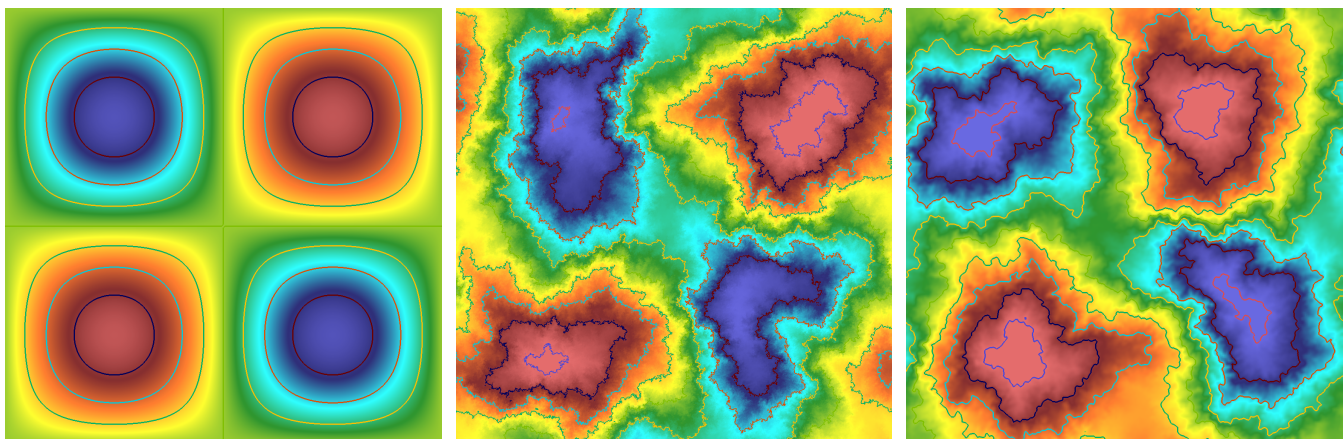

Figure 2: The concentration obtained after a substantial decay of a single-mode initial condition $c(\boldsymbol{r}, 0) = \sin(2\pi x/L)\sin(2\pi y/L)$. Contour lines are also shown, and the same final time $t \sim \tau$ and color legend is used in all three panels. (*Left panel*) The ensemble averaged mean, which follows (11). (*Middle*) Solution of the stochastic advection-diffusion equation (5) on a grid of size 1024×1024 cells for the case $\chi_{\text{eff}}/\chi_0 \approx 50$. (*Right panel*) An instance of the solution of (5) for a grid of size 256×256 cells, for $\chi_{\text{eff}}/\chi_0 \approx 5$, with the same $\chi_{\text{eff}} = \chi_0 + \chi$ as the other two panels.

To this end, let us consider the temporal decay of a smooth single-mode initial perturbation $c(\boldsymbol{r}, 0) = \sin(2\pi x/L)\sin(2\pi y/L)$ in two dimensions, using our numerical method for simulating the overdamped dynamics (5,9). In the left panel of Fig. 2, we show the ensemble mean of the concentration at a later time, as obtained by solving the deterministic equation (11) with an effective diffusion coefficient $\chi_{\text{eff}} = \chi_0 + \chi$, where the value of χ was obtained via the discrete equivalent of (13). In the middle panel of the figure, we show an instance of the concentration at the same time obtained by solving (5,9) using the smallest value of χ_0 that stabilized the numerical scheme. The same giant fluctuations seen in Fig. 1 are revealed, with the contour lines of the concentration becoming rough even at the scale of the grid spacing. We note in passing that we have performed hard-disk molecular dynamics simulation of this mixing process and have observed the same qualitative behavior seen in the middle panel of Fig. 2.

A. Power Transfer

The conserved quantity[5] $\int \left(c^2/2\right) d\boldsymbol{r}$ injected via the initial perturbation away from equilibrium is effectively dissipated through a mechanism similar to the energy cascade observed in turbulent flows. Advection transfers power from the large length scales to the small length scales, *effectively* dissipating the power injected into the large scales via the initial condition. To make this more quantitative, let us set $\chi_0 = 0$ and write (5) in the Fourier domain,

$$\frac{d\hat{c}_{\boldsymbol{k}}}{dt} = \hat{\boldsymbol{w}}_{\boldsymbol{k}} \circledast \left(i\boldsymbol{k}\hat{c}_{\boldsymbol{k}}\right),$$

where $\circledast$ is a combination of Stratonovich dot product and convolution. This equation strictly conserves the total power $\sum_{\boldsymbol{k}} \left|\hat{c}_{\boldsymbol{k}}\left(t\right)\right|^2 /2$ since the advective term simply redistributes the power between the modes. Let us denote the ensemble average power in mode $\boldsymbol{k}$ with $p_{\boldsymbol{k}}\left(t\right) = \langle\left|\hat{c}_{\boldsymbol{k}}\left(t\right)\right|^2\rangle/2$. Using straightforward stochastic calculus we can obtain a simple system of ODEs for the transfer of power between the modes,

$$\frac{dp_{\boldsymbol{k}}}{dt} = -\sum_{\boldsymbol{k}'\neq\boldsymbol{k}} \left(\boldsymbol{k} \cdot \hat{\boldsymbol{\chi}}_{\boldsymbol{k}-\boldsymbol{k}'} \cdot \boldsymbol{k}\right) p_{\boldsymbol{k}} + \sum_{\boldsymbol{k}'\neq\boldsymbol{k}} \left(\boldsymbol{k}' \cdot \hat{\boldsymbol{\chi}}_{\boldsymbol{k}-\boldsymbol{k}'} \cdot \boldsymbol{k}'\right) p_{\boldsymbol{k}'}. \tag{20}$$

The first term on the right hand side of this equation expresses the power lost from mode $\boldsymbol{k}$ to other modes, while the second term gives the power transferred from other modes to mode $\boldsymbol{k}$. The total power $\sum_{\boldsymbol{k}} p_{\boldsymbol{k}}$ is conserved because the flow in (16) is unique, ensuring that there is no anomalous dissipation [52].

Consider starting from an initial configuration in which the only mode with nonzero power is wavenumber $\boldsymbol{k}_0$, $\hat{c}_{\boldsymbol{k}}\left(0\right) = \delta_{\boldsymbol{k},\boldsymbol{k}_0}$. The average rate at which power will be transferred from mode $\boldsymbol{k}_0$ to mode $\boldsymbol{k} \neq \boldsymbol{k}_0$ via the advective term $-\boldsymbol{w} \odot \boldsymbol{\nabla}c$ is proportional to the spectrum of $\boldsymbol{w}$ at wavenumber $\boldsymbol{k} - \boldsymbol{k}_0$ and is given by $\boldsymbol{k}_0 \cdot \hat{\boldsymbol{\chi}}_{\boldsymbol{k}-\boldsymbol{k}_0} \cdot \boldsymbol{k}_0$. The total relative rate at which power is lost ("dissipated") from mode $\boldsymbol{k}_0$ is given by $\boldsymbol{k}_0 \cdot \boldsymbol{\chi} \cdot \boldsymbol{k}_0$, where $\boldsymbol{\chi} = \sum_{\boldsymbol{k}} \hat{\boldsymbol{\chi}}_{\boldsymbol{k}}$ for a finite system case, or $\boldsymbol{\chi} = \left(2\pi\right)^{-d} \int \hat{\boldsymbol{\chi}}_{\boldsymbol{k}} d\boldsymbol{k}$ in the infinite system limit. This is exactly the same rate of dissipation as one would get for ordinary diffusion with diffusion tensor $\boldsymbol{\chi}$. In simple diffusion, the power of mode $\boldsymbol{k}_0$ would also decay exponentially as $\exp\left(-t/\tau\right)$, where $\tau = \left(2\chi_{\text{eff}}k_0^2\right)^{-1}$ is a decay time. However, all other modes would remain unexcited, as in the left panel of Fig. 2.

The above calculation shows that after a short time $t \ll \tau$, mode $\boldsymbol{k} \neq \boldsymbol{k}_0$ will have, on average, power proportional to $\left(\boldsymbol{k}_0 \cdot \hat{\boldsymbol{\chi}}_{\boldsymbol{k}-\boldsymbol{k}_0} \cdot \boldsymbol{k}_0\right) t$. For large-scale initial perturbations, $\boldsymbol{k}_0 \approx \boldsymbol{0}$, the spectrum of c at short times will therefore be proportional to one of the diagonal elements of $\hat{\boldsymbol{\chi}}_{\boldsymbol{k}}$, which can be read from (14) to be $\sim k^{-2}\sin^2\theta$ for intermediate wavenumbers, where θ is the angle between $\boldsymbol{k}$ and $\boldsymbol{k}_0$. The spectrum at early times is therefore $\left|\hat{c}_{\boldsymbol{k}}\left(t\right)\right|^2 \sim k^{-2}t$, as confirmed by our numerical simulations and illustrated in Fig. 3.

If there were only random advection, with no bare diffusion, the transfer of energy from the coarse to the fine scales would continue indefinitely. It is not hard to see that even a very small finite bare diffusion can affect the results at small scales dramatically, making the limit $\chi_0 \to 0^+$ non-trivial [53]. Namely, the diffusive term $\chi_0 \boldsymbol{\nabla}^2 c$ becomes stronger and stronger at smaller scales ($\chi_0 k^2$ in Fourier space), and will eventually become important and dissipate the small scale features created by the random advection. In particular, at late times of the diffusive decay, $t \sim \tau$, shown in Fig. 2, one expects that a steadily decaying state will be reached in which the shape of the spectrum of c does not change as it decays exponentially in time as $\exp\left(-t/\tau\right)$. This is indeed what we observe, and the shape of the steadily decaying spectrum is shown in Fig. 3. Numerically we observe that the majority of the bare dissipation occurs at the largest wavenumbers, dissipating the power injected into small scales from the large and intermediate scales. This is seen in Fig. 3 as a deviation from the power-law behavior for the largest wavenumbers. It is important to note that the shape of the spectrum at the large wavenumbers is strongly affected by discretization artifacts for the finite volume scheme employed here.

We also study the spectrum of concentration fluctuations with the Lagrangian tracer algorithm described in Section II D, which allows us to eliminate bare diffusion and numerical grid artifacts. Note however that the Lagrangian approach to obtaining power spectra also fails at sufficiently large wavenumbers at sufficiently large times, as we explain shortly. In the Lagrangian algorithm, we make use of the time-reversibility of the flow, $c\left(\boldsymbol{q}(0), t\right) = c\left(\boldsymbol{q}(t), 0\right)$. We place $N_t = 2048^2$ on a regular grid at the initial time and then follow their trajectories over a time interval t using the algorithm described in Section B 2. We then evaluate the initial condition $c\left(\boldsymbol{r}, 0\right)$ at the final position of each tracer in order to obtain the concentration $c\left(\boldsymbol{r}, t\right)$ on a regular

---

[5] Advection preserves not just the second but all moments of the concentration.
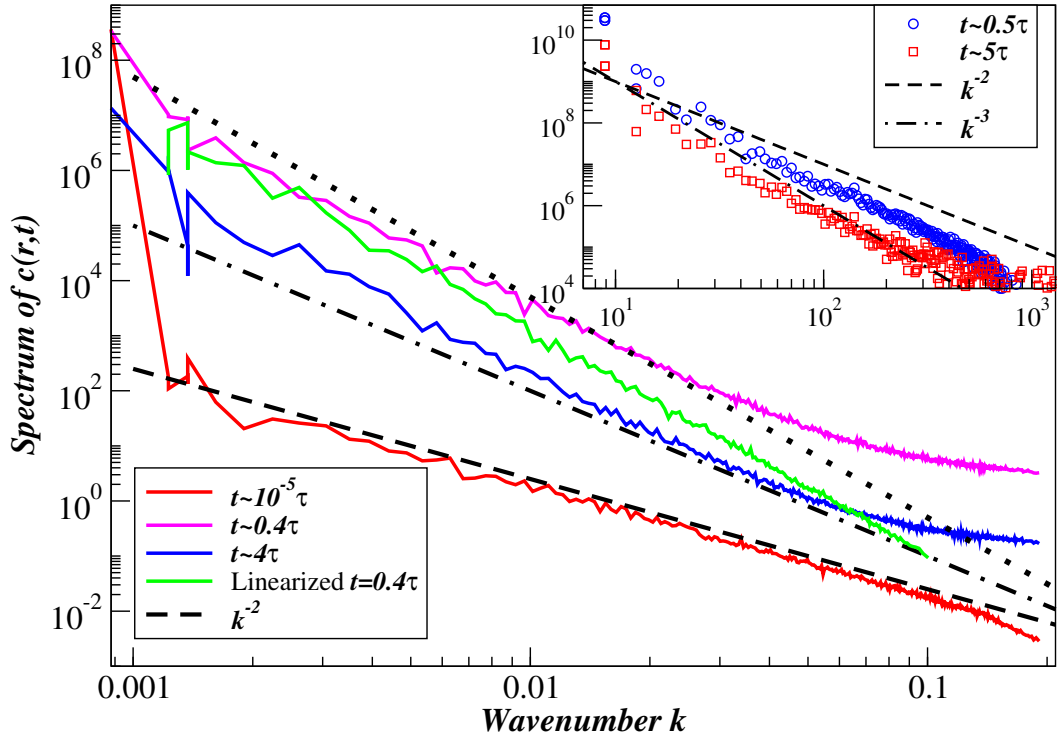
Figure 3: Power spectrum of an *individual* realization of the concentration $c(\boldsymbol{r}, t)$ corresponding to the simulation illustrated in the middle panel in Fig. 2. The power of individual modes $\boldsymbol{k}$ with nearby k is averaged and the result is shown with a colored solid line, while dashed/dotted lines show power laws k^{-2}, k^{-3} and k^{-4} for comparison. At early times $t \ll \tau = \left(2\chi_{\text{eff}}k_0^2\right)^{-1}$ (red line) power is being transferred from mode $k_0 \approx 2\pi/L \approx 10^{-3}$, initially excited to have spectral power $p_{\boldsymbol{k}_0} \approx 7 \cdot 10^8$ (off scale), to the rest of the modes, leading to a spectrum $\sim k^{-2}$. At late times $t \gtrsim \tau$ (magenta and blue lines), a steadily-decaying shape of the spectrum is reached where power transferred from the larger scales is dissipated at the small scales via bare diffusion. Linearized fluctuating hydrodynamics predicts a spectrum $\sim k^{-4}$ (green line). (*Inset*) Difference in the spectrum between random advection and simple diffusion, as obtained using a Lagrangian simulation of the diffusive decay. The parameters used are different from the main panel and are summarized in Section IV.

grid of points, and use the FFT algorithm to obtain the spectrum $\hat{c}_{\boldsymbol{k}}(t)$. This would be a very accurate numerical algorithm if the concentration were smooth on the scale of the grid of tracers. In reality, as the power-law tail in the spectrum gets filled by the advection the concentration becomes less and less smooth and the spectrum at the larger wavenumbers becomes dominated by truncation errors (using a discrete sum instead of a Fourier integral) and statistical errors (using a finite number of sampling points to obtain the spectrum).

In order to eliminate these artifacts and further emphasize the difference between simple diffusion and advection by a random field, we consider repeating the Lagrangian calculation with tracers that perform *independent* Brownian motions with diffusion coefficient χ_{eff}. For simple diffusion, the numerical spectrum is not zero for $\boldsymbol{k} \neq \boldsymbol{k}_0$ as it should be; rather, due to the finite number of tracers we get $p_{\boldsymbol{k}}(t) \sim N^{-1}[1 - \exp(-t/\tau)]$. We subtract this background noise from the numerical spectrum obtained using the Lagrangian tracing algorithm. We find that the difference in the spectrum for random advection and simple diffusion follows a power-law behavior, as illustrated in the inset of Fig. 3. The power law is in agreement with that seen in the Eulerian simulations, and persists over the whole range of accessible wavenumbers.

B. Linearized Fluctuating Hydrodynamics

In the literature, linearized fluctuating hydrodynamics is frequently used to obtain the steady-state spectrum of fluctuations [3]. In the limit of large Schmidt numbers, the standard heuristic approach leads to the additive-noise equation,

$$\partial_t \tilde{c} = -\boldsymbol{w} \cdot \boldsymbol{\nabla}\langle c \rangle + \boldsymbol{\nabla} \cdot [\chi_{\text{eff}} \boldsymbol{\nabla}\tilde{c}], \tag{21}$$

where $\langle c \rangle$ is the ensemble mean, which follows (11). Note that in order to obtain the correct spectrum for the *equilibrium* concentration fluctuations, one ought to include an additional random forcing term $\boldsymbol{\nabla} \cdot \left(\sqrt{2\chi_{\text{eff}}\langle c \rangle}\, \boldsymbol{\mathcal{W}}_c \right)$ in (21); our focus here is on the *nonequilibrium* fluctuations and we will not include such a term to more accurately measure the power-law spectrum. Equation (21) can easily be solved analytically in the Fourier domain when $\boldsymbol{\nabla}\langle c \rangle = \boldsymbol{h}$ is a weak externally applied constant gradient (c.f., for example, Eq. (9) in Ref. [9]), to obtain a spectrum $(\boldsymbol{h} \cdot \hat{\boldsymbol{\chi}}_{\boldsymbol{k}} \cdot \boldsymbol{h})/(\chi_{\text{eff}}k^2) \sim k^{-4}$ for intermediate wavenumbers.

Linearized fluctuating hydrodynamics can be used to justify the omission of the term $\boldsymbol{\nabla} \cdot \left(\sqrt{2\chi_0 c}\, \boldsymbol{\mathcal{W}}_c \right)$ from (4) in our numerical calculations. This term leads to "equilibrium" concentration fluctuations that are negligible compared to the "non-equilibrium" concentration fluctuations due to advection by the thermal velocity fluctuations in the presence of large concentration gradients. A rough estimate of the magnitude of the equilibrium versus the nonequilibrium fluctuations can be obtained by considering the case when the tracer particles are labeled molecules of a simple three-dimensional liquid with molecular mass m, molecular diameter σ and molecular number density $n = \rho/m \sim \sigma^{-3}$. The spectrum of the equilibrium fluctuations is $\langle |\hat{c}_{\boldsymbol{k}}|^2 \rangle_{\text{eq}} \approx \langle c \rangle \sim \phi \sigma^{-3}$, where ϕ is the volume (packing) fraction of the labeled particles. In the presence of a constant applied concentration gradient of magnitude h, an additional nonequilibrium contribution $\langle |\hat{c}_{\boldsymbol{k}}|^2 \rangle_{\text{neq}} \approx h^2 n^2 k_B T/(\eta \chi_{\text{eff}} k^4)$ is obtained (see Appendix A in Ref. [31], but note that in that work c denotes mass fraction, rather than number concentration as it does in this paper). To estimate the ratio of these two contributions we can use the Stokes-Einstein relation $\chi_{\text{eff}} \sim k_B T/(\eta \sigma)$ and $h \sim L^{-1}$, where $L \gg \sigma$ is the scale of the applied gradient, to obtain

$$\langle |\hat{c}_{\boldsymbol{k}}|^2 \rangle_{\text{eq}}/\langle |\hat{c}_{\boldsymbol{k}}|^2 \rangle_{\text{neq}} \sim \phi \, L^2 \sigma^2 k^4.$$

At length scales $k \sim L^{-1}$, the above ratio is $\sim (\sigma/L)^2 \ll 1$, and in practical situations the nonequilibrium fluctuations are "giant" compared to the equilibrium ones.

For finite gradients and more realistic boundary conditions, we can solve (21) numerically with the same algorithm used to solve the full nonlinear equation (5). Namely, we set $\chi_0 = \chi_{\text{eff}}$ and reduce the magnitude of the fluctuations by a factor $\epsilon \ll 1$ by setting the "temperature" to $\epsilon k_B T$, and then simply rescale the spectrum of the fluctuations by a factor ϵ^{-1} to obtain the spectrum of $\tilde{c}$. This approach was used by some of us to simulate giant concentration fluctuations in microgravity [6] in Ref. [29]. The result of this numerically-linearized calculation for the single-mode initial condition is shown in Fig. 3 and compared to the nonlinear calculations. The spectrum is indeed seen to follow a power-law k^{-4} for the linearized equations, in agreement with theory. Note however that the spectrum obtained from (21) is not in a very good match with the spectrum obtained by solving (5), which appears closer to k^{-3} in the two-dimensional setting we study here. Tools developed in the turbulence literature [35, 36] could potentially be used to study the spectrum of uniformly decaying steady states without resorting to linearization. Alternatively, the system of differential equations (20) can be solved numerically to study the average dynamics of the transfer of power between the modes.

By integrating the $\sim k^{-4}$ spectrum of concentration fluctuations predicted by (21) it can easily be seen that in two dimensions the fluctuations of the concentration around the Fickian mean are on the order of the applied concentration gradient. Therefore, they *cannot* be considered "microscopic" or "small", and linearized fluctuating hydrodynamics does *not* apply in two dimensions. For example, the solution of (21) does not necessarily stay positive due to the large fluctuations, as we have observed numerically for parameters representative of moderately-dense hard-disk systems. This is an inherent pitfall of linearizing the nonlinear advective term when fluctuations become truly "giant" (as they do in two dimensions). By contrast, the nonlinear equations preserve the bounds on concentration even when the fluctuations become strong, since advecting by a spatially smooth (even if white in time) velocity obeys a monotonicity principle.

IV. Spatial Coarse-Graining

If there were only random advection, with no bare diffusion, the transfer of energy from the coarse to the fine scales would continue indefinitely, since the dynamics is reversible and there is nothing to dissipate the power. However, any features in c at length scales below molecular scales have no clear physical meaning. In fact, continuum models are inapplicable at those scales. It is expected that not resolving (coarse-graining) the microscopic scales will lead to true dissipation and irreversibility in the coarse-grained dynamics. Such coarse-graining can take form of ensemble averaging, or elimination of slow degrees of freedom. In either case, the loss of knowledge about the small scales will lead to positive entropy production.

Can one replace the molecular scale details, or even all details of the dynamics at scales below some mesoscopic observation scale δ, by some simple approximation, for example, a bare diffusion term with suitably chosen χ_0? We propose here a way to carry out such *spatial* coarse-graining of the overdamped

dynamics (5,9) by splitting the velocity $\boldsymbol{w}$ into a large-scale component $\boldsymbol{w}_\delta$ and a small-scale component $\tilde{\boldsymbol{w}}$,

$$\boldsymbol{w} = \boldsymbol{\delta} \star \boldsymbol{w} + \tilde{\boldsymbol{w}} = \boldsymbol{w}_\delta + \tilde{\boldsymbol{w}},$$

where $\boldsymbol{\delta}$ is a filter that smooths scales below some mesoscopic length $\delta > \sigma$. More precisely, the equality $\boldsymbol{w} = \boldsymbol{w}_\delta + \tilde{\boldsymbol{w}}$ is in law and corresponds to splitting the covariance matrix $\boldsymbol{\mathcal{R}} = \boldsymbol{\delta} \star \boldsymbol{\mathcal{R}} \star \boldsymbol{\delta}^T + \widetilde{\boldsymbol{\mathcal{R}}}$ into a small-scale and large-scale component, and generating the two parts of $\boldsymbol{w}$ independently. Because of the technical difficulty in dealing with the multiplicative noise term $\boldsymbol{\nabla} \cdot \left(\sqrt{2\chi_0 c}\, \boldsymbol{\mathcal{W}}_c \right)$ in (9), we do not include this term in this analysis.

In Eq. (11), we performed an ensemble average over all realizations of $\boldsymbol{w}$. We can also, however, only average over realizations of the unresolved $\tilde{\boldsymbol{w}}$, that is, we can define $\bar{c}_\delta = \langle c \rangle_{\tilde{\boldsymbol{w}}}$ as the conditional ensemble average keeping $\boldsymbol{w}_\delta$ fixed. We can directly take such a conditional average of the Ito equation (9), to obtain, *without* any approximations, a closed equation for $\bar{c}_\delta$ of exactly the same form as (9),

$$\partial_t \bar{c}_\delta = -\boldsymbol{w}_\delta \cdot \boldsymbol{\nabla} \bar{c}_\delta + \chi_0 \boldsymbol{\nabla}^2 \bar{c}_\delta + \boldsymbol{\nabla} \cdot \left[\boldsymbol{\chi} \left(\boldsymbol{r} \right) \boldsymbol{\nabla} \bar{c}_\delta \right], \tag{22}$$

with exactly the same initial condition, and, importantly, with an identical effective diffusion coefficient $\chi_{\text{eff}} = \chi_0 + \boldsymbol{\chi}$. However, if we write (22) in the Stratonovich form used by our numerical methods, we see that the bare diffusion coefficient needs to be *renormalized* to take into account the coarse-grained scales,

$$\partial_t \bar{c}_\delta = -\boldsymbol{w}_\delta \odot \boldsymbol{\nabla} \bar{c}_\delta + \boldsymbol{\nabla} \cdot \left[\left(\chi_0 + \Delta \boldsymbol{\chi}_\delta \right) \boldsymbol{\nabla} \bar{c}_\delta \right], \tag{23}$$

where the diffusion renormalization $\Delta \boldsymbol{\chi}_\delta$ is

$$\Delta \boldsymbol{\chi}_\delta \left(\boldsymbol{r} \right) = \frac{1}{2} \widetilde{\boldsymbol{\mathcal{R}}} \left(\boldsymbol{r}, \boldsymbol{r} \right) = \frac{1}{2} \boldsymbol{\mathcal{R}} \left(\boldsymbol{r}, \boldsymbol{r} \right) - \frac{1}{2} \int \boldsymbol{\delta} \left(\boldsymbol{r}, \boldsymbol{r}' \right) \boldsymbol{\mathcal{R}} \left(\boldsymbol{r}', \boldsymbol{r}'' \right) \boldsymbol{\delta}^T \left(\boldsymbol{r}, \boldsymbol{r}'' \right) d\boldsymbol{r}' d\boldsymbol{r}'' \tag{24}$$

Note that the renormalized *bare* diffusion coefficient $\chi_0 \left(\delta \right) = \chi_0 + \Delta \boldsymbol{\chi}_\delta$ in (23) is nonzero even if $\chi_0 = 0$. This true dissipation is a remnant of the unresolved (eliminated) small scales. This renormalized bare diffusion coefficient is not, however, a material constant, but rather, depends on the mesoscopic lengthscale δ.

A. Coarse-Grained Stochastic Advection-Diffusion Model

In reality, we are not interested in the behavior of the conditional average $\bar{c}_\delta$ because this is not a measurable quantity. Rather, we are interested in the behavior of individual realizations of the spatially coarse-grained concentration $c_\delta = \boldsymbol{\delta} \star c$, which can be measured by observing c at scales larger than some experimental resolution δ. A physically reasonable coarse-grained model can be obtained by *assuming* that c_δ follows the same equation as the conditional mean $\bar{c}_\delta$,

$$\partial_t c_\delta \approx -\boldsymbol{w}_\delta \odot \boldsymbol{\nabla} c_\delta + \boldsymbol{\nabla} \cdot \left[\left(\chi_0 + \Delta \boldsymbol{\chi}_\delta \right) \boldsymbol{\nabla} c_\delta \right], \tag{25}$$

so long as the initial condition is smooth [6] at the scale δ. It is important to note that, in order to obtain correct equilibrium fluctuations, there should also be an additional stochastic forcing term in (25). This term would balance the enhanced bare dissipation and restore fluctuation-dissipation balance in the coarse-grained system [23]. A suitable form of this term is not obvious and we do not include this term here just as we did not include the stochastic forcing term $\boldsymbol{\nabla} \cdot \left(\sqrt{2\chi_0 c}\, \boldsymbol{\mathcal{W}}_c \right)$.

It is not possible to numerically solve (5) due to the presence of nontrivial dynamics at essentially *all* length scales, especially in the absence of bare diffusion. Our arguments suggest that we can instead solve the coarse-grained equation (25), which has exactly the same form as (5), but in which small scales are not resolved, and there is increased bare dissipation. This is very easy to do in finite-volume numerical methods for solving (5) by simply increasing the cell volume and increasing the bare diffusion coefficient accordingly. In the right panel of Fig. 2, we show the result of an Eulerian simulation performed with a four times coarser grid than the middle panel. This is roughly equivalent to choosing $\delta = 4\sigma$ and solving (25). The value of χ_0 is increased according to a discrete equivalent of (24) to account for the unresolved scales. This ensures that the effective diffusion coefficient χ_{eff} is the same for all panels of Fig. 2, in agreement with (22). Except at scales not resolved by the four-times coarser grid, the right panel and the middle panel look similar visually, as confirmed by an examination of the corresponding Fourier spectra. This suggests that (25) is indeed a good approximation to the true dynamics of the spatially coarse-grained concentration. A more quantitative comparison between the spatially smoothed c_δ and the conditional average $\bar{c}_\delta$ will be performed in future studies.

We emphasize that the inclusion of the fluctuating term $-\boldsymbol{w}_\delta \odot \boldsymbol{\nabla} c_\delta$ in (25) is *necessary* to obtain the correct physical behavior, especially in two dimensions. In large three dimensional systems, when the spatial coarse-

---

[6] One can also use initial condition $c_\delta(0) = \boldsymbol{\delta} \star c(0)$ since the enhanced bare diffusion quickly damps fine-scale features in the initial condition.

graining is performed at macroscopic scales $\delta \gg \sigma$, it has often been assumed [3] that one can approximate (25) with the deterministic Fick's law (11) and linearize the fluctuations around the deterministic dynamics, as in (21). To our knowledge there have been no precise mathematical arguments to support this picture suggested by renormalization arguments [7]. In two dimensions, linearization is certainly not appropriate due to the logarithmic growth of the effective diffusion coefficient (15) with system size. Thin films may exhibit an intermediate behavior depending on the scale of observation relative to the thickness of the thin film [54].

B. Irreversibility of Coarse-Graining

In the coarse-grained dynamics (25), there is irreversible dissipation, $\Delta\chi_\delta > 0$, even in the absence of dissipation in the original dynamics. It is easy to appreciate that elimination of degrees of freedom (coarse-graining) is necessary in order to obtain dissipative (irreversible) dynamics starting from a non-dissipative (reversible, even Hamiltonian) dynamics [23]. Consider the specific example of diffusive mixing illustrated in Fig. 1 in the absence of bare diffusion, $\chi_0 = 0$. Since $\boldsymbol{u}$ and $\boldsymbol{w}$ are spatially-smooth velocity fields, advection by $\boldsymbol{u}$ or $\boldsymbol{w}$, in the absence of bare diffusion, leads to behavior qualitatively different from diffusion. Specifically, if the initial concentration $c(\boldsymbol{r}, 0)$ has a sharp interface, this interface will remain sharp at all times, even if it becomes very rough. This implies that if $\chi_0 = 0$, in Fig. 1 one should see only the red and blue colors present in the initial snapshot, at *all* times, in *every* realization, instead of the spectrum of colors actually seen in the figure.
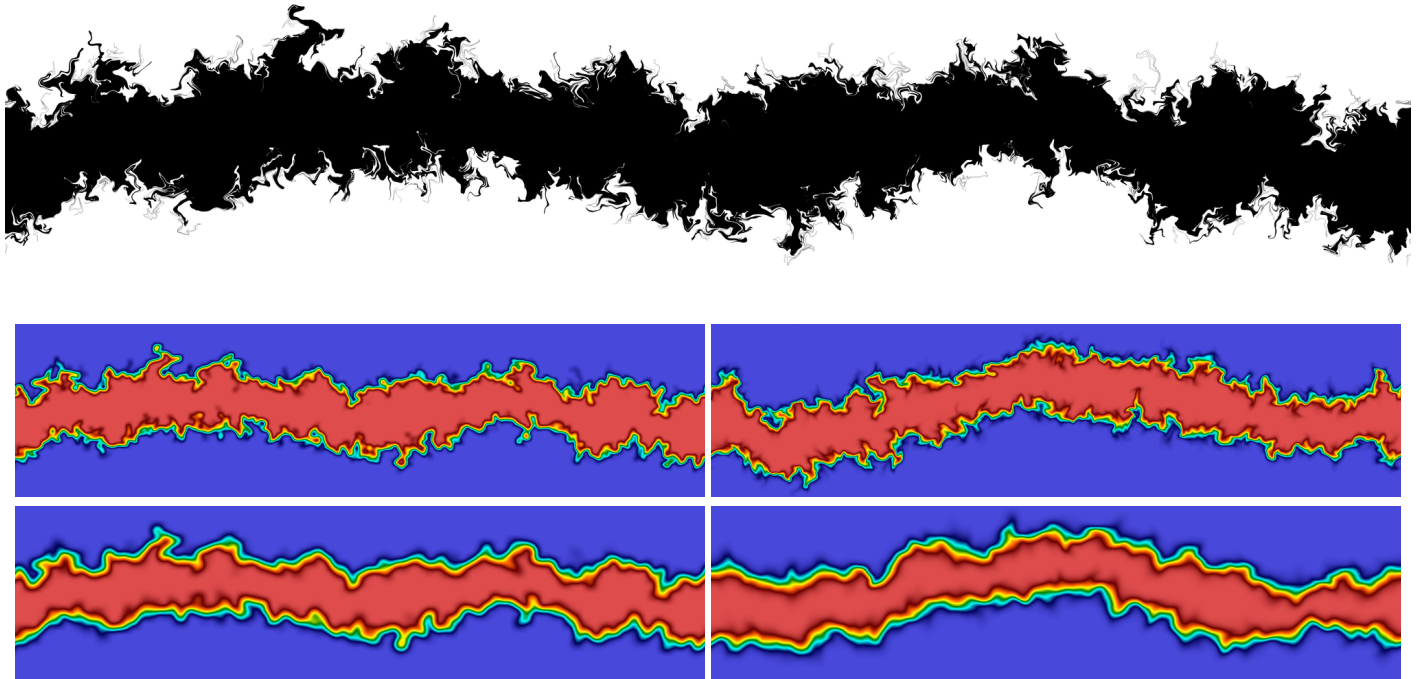

Figure 4: (*Top panel*) A snapshot of the concentration c for the diffusive mixing process first shown in Fig. 1, here in the absence of bare diffusion, $\chi_0 = 0$. The top and bottom interface are represented with about half a million Lagrangian tracers each, and (16) is solved for each tracer numerically. A Gaussian filter with standard deviation σ is used to filter the velocity field, and the periodic domain has unit cell of shape $512\sigma \times 128\sigma$. The space between the two interfaces is colored black using image-processing tools. (*Two color panels on left*) The spatially-coarse grained concentration c_δ obtained by blurring the top panel using a Gaussian filter with standard deviation δ, for $\delta = 1.5\sigma$ (top left) and $\delta = 3\sigma$ (bottom left). (*Two color panels on right*) An independent snapshot of the conditional average $\bar{c}_\delta$ at the same point in time as the panels on the left, obtained by solving (23) with an Eulerian method using a grid of 2048×512 finite-volume cells. A Gaussian filter of width δ is used to filter the discrete velocity and the bare diffusion χ_0 is chosen such that χ_{eff} is the same as in the Lagrangian simulations. In the top panel, $\delta = 1.5\sigma$ (six grid cells) and $\chi_{\text{eff}}/\chi_0 \approx 9.6$, and in the bottom panel $\delta = 3\sigma$ and $\chi_{\text{eff}}/\chi_0 \approx 3.5$. The same settings and random number sequence was used to generate the random velocities for both panels on the right in order to facilitate a direct comparison.

We turn to our Lagrangian tracer algorithm for solving (16) as a means to track the interface in Fig. 1 without dissipation. For the particular example of diffusive mixing starting from a sharp interface, in the absence of

bare diffusion, tracking the interface is sufficient to reconstruct the solution everywhere. Specifically, $c = 0$ on one side of the interface (topologically a closed curve on the torus for a periodic system), and $c = 1$ on the other side. Therefore, we put a large number of Lagrangian tracers on the flat interface at $t = 0$, keeping the distance between neighboring tracers much smaller than the tracer/molecular cutoff scale σ. We then simulate a realization of the particles' trajectories to a later time, connecting neighboring points with straight line segments to obtain an approximation of the interface. In the top panel of Fig. 4 we show the results of a Lagrangian simulation of the mixing process first illustrated in Fig. 1. The top and bottom interface are tracked using tracers, and the concentration in the space between the two interfaces is set to $c = 1$ (black), $c = 0$ elsewhere (white).
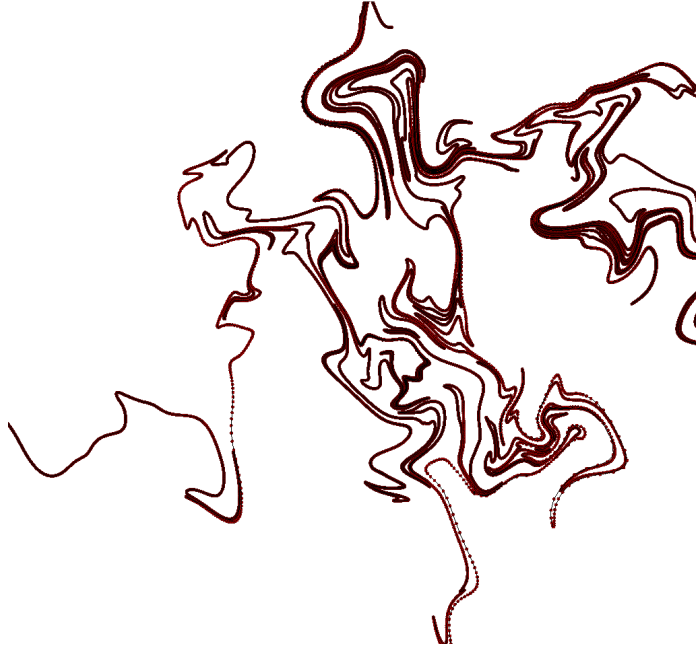

Figure 5: A snapshot of a portion of an initially straight line of Lagrangian tracers after some time. The individual tracers and the straight line segments connecting them are both shown. The length of the shown portion of the domain is about 20σ.

As illustrated in Fig. 5, an initially straight line of tracers becomes quite contorted at later times, even though topologically it remains a non-crossing curve at all times. Asymptotically as $t \to \infty$ we expect that the line will densely cover the plane (i.e., become a space-filling curve), in the same way that simple diffusion would lead to uniform concentration throughout the domain. Simulating the mixing process using a Lagrangian algorithm would therefore require an unbounded increase in the number of Lagrangian tracers with time in order to track the ever-increasing level of fine-scale detail in the interface. Spatial coarse-graining introduces effective bare diffusion and eliminates the fine-scale details in the mixing front. In the two color panels on the left in Fig. 4 we show the concentration field $c_\delta = \boldsymbol{\delta} \star c$ smoothed with a Gaussian filter of width $\delta = 1.5\sigma$ and $\delta = 3\sigma$, now showing a spectrum of colors due to the spatial averaging.

In the two color panels on the right in Fig. 4 we show statistically-independent samples of the conditional average $\bar{c}_\delta = \langle c \rangle_{\tilde{\boldsymbol{w}}}$ obtained by solving (23) using a finite-volume Eulerian algorithm. A slight modification of the algorithm used to prepare Figs. 1, 2 and 3 was implemented, in which the discrete random advection velocity $\boldsymbol{w}$ was filtered in Fourier space with a Gaussian filter of width δ to obtain the $\boldsymbol{w}_\delta$, as discussed in more detail in Section B 1. The grid spacing was set to be smaller than $\delta/6$, which ensures that discretization artifacts are quite small and the Eulerian code can be directly compared to the very accurate Lagrangian code. The value of the coarse-graining length was set to be $\delta > \sigma$, and the bare diffusion coefficient $\Delta\chi_\delta > 0$ was set so that the effective diffusion coefficient χ_{eff} remained the same as in the Lagrangian simulation. One can choose the balance between bare diffusion and enhanced diffusion essentially arbitrarily by choosing the length scale δ at which to truncate (filter) the velocity spectrum, and for the top right color panel of the figure we used the smallest value of $\delta = 1.5\sigma$ that stabilized the numerical method. The coarse-graining length $\delta = 3\sigma$ is twice larger in the bottom right color panel than in the top right color panel, and therefore there is enhanced bare diffusion

(smoothing). Visually the two color panels on the left and on the right in Fig. 4 look quite similar. This indicates that (25) gives a good approximation to the nonequilibrium fluctuations in the coarse-grained field c_δ.

C. A Paradigm for Diffusion

Let us now summarize our discussion of spatial coarse-graining. We start from the overdamped equation (5) as the most accurate representation of diffusion, although itself an approximation of the true molecular transport processes. The reference molecular scale σ and bare diffusion coefficient χ_0 may in principle be extracted from comparisons to a more fundamental model such as molecular dynamics, or from experimental observations. In the end, the precise details of the dynamics at the molecular scale do not matter, since at the larger scales they only enter through a renormalized bare diffusion coefficient. In fact, the microscopic equation (5) should never be solved directly. Doing so numerically would require using a grid resolution smaller than the molecular scale, and, in the case of no bare diffusion, would require an infinite resolution due to the creation of every finer-scale details in the solution even when the initial condition is smooth. Instead, what one should really calculate is the spatially-coarse grained $c_\delta = \boldsymbol{\delta} \star c$, where $\delta \gg \sigma$ is a scale of observation.

In order to derive an approximation for the dynamics of c_δ, we started by splitting the spectrum of the velocity fluctuations into a microscopic component $\tilde{\boldsymbol{w}}$ containing the fluctuations at scales below a mesoscopic length δ, and the rest of the spectrum extending all the way to the macroscopic scale. A rigorous closed-form equation for the conditional average $\bar{c}_\delta = \langle c \rangle_{\tilde{\boldsymbol{w}}}$ is given by (23). A key result of our numerical experiments illustrated in Fig. 4 is that $c_\delta \approx \bar{c}_\delta$, more precisely, that (23) can be used to approximate the uknown dynamics of c_δ. We can express the relations between the different quantities by the following diagram

$$c_\delta = \boldsymbol{\delta} \star c$$

$$c \qquad \qquad \Updownarrow$$

$$\bar{c}_\delta = \langle c \rangle_{\tilde{\boldsymbol{w}}}$$

In the coarse-grained approximation (25), the bare diffusion coefficient is renormalized to take into account the contribution of advection by the unrepresented (eliminated) velocity scales. This makes solving this equation numerically a much simpler task, since the enhanced bare diffusion dissipates small scale features in the solution.

The correspondence $c_\delta \Leftrightarrow \bar{c}_\delta$ is an approximation inspired by (23). Stochastic homogenization theory [11] can potentially be used to justify (25) for $\delta \gg \sigma$. It is unlikely that there can be a rigorous justification for this identification in the case when there is no separation of scales between the mesoscopic and microscopic scales, i.e., when $\delta \sim \sigma$, even though Fig. 4 shows a very good visual agreement. In future work we will perform more detailed quantitative comparisons in order to quantify the length and time scales at which (25) is a good approximation.

V. Conclusions

We presented a model of diffusion in liquids that captures in a simple yet precise way the contribution that thermal velocity fluctuations make to the transport of a passive tracer. The standard equations of fluctuating hydrodynamics used to describe the effect of thermal fluctuations on diffusion [3] need to be regularized below a cutoff molecular scale. We introduced this regularization by filtering the fluctuating velocity field $\boldsymbol{v}$ at a molecular scale σ in order to obtain a smooth (in both space and time) velocity $\boldsymbol{u}$ with which we advect the passive tracer. Under the assumption of large separation of scales between the fast momentum diffusion (collisional transport of momentum) and the slow mass diffusion, i.e., large Schmidt number, we obtained an overdamped limiting equation for the concentration. This equation is amenable to numerical simulations, allowing us to simulate diffusive mixing even in the presence of infinite separation of time scales between mass and momentum diffusion.

In the Stratonovich form the overdamped equation for the concentration of passive tracers is a stochastic advection-diffusion equation in which the thermal velocity fluctuations enter as a white-in-time random advection field $\boldsymbol{w}$ with spectrum given by a Green-Kubo formula. For the case of Stokes flow the spectrum of $\boldsymbol{w}$ is proportional to a regularized Oseen tensor. In the Ito form of the overdamped equation, there is an additional diffusive term with diffusion coefficient closely related to the Stokes-Einstein prediction for the diffusion coefficient of a sphere of radius σ immersed in the fluid. This enhancement of the diffusion over the bare diffusion is mathematically similar to the well-known eddy diffusivity in turbulent transport. However, its origin is very different physically since the random flow here describes very low Reynolds number thermal fluctuations in the velocity. Unlike previous derivations of the Stokes-Einstein law for diffusion in liquids, our model makes no

assumptions beyond that of a large Schmidt number and gives a stochastic *dynamical* description of diffusion.

The sum of the bare and enhanced diffusion coefficients determines the effective diffusion coefficient, which gives the rate of dissipation in the ensemble mean. In each individual realization of the diffusion process, however, bare diffusion and the random advection giving rise to the enhanced diffusion behave rather differently because the random advection is strictly non-dissipative. We showed that, from the perspective of an initially excited mode (wavenumber), the advection by the random velocity field effects apparent dissipation in the form of transfer of power into other modes. The average rate of power dissipation is found to be exactly the same as for simple diffusion with an equal effective diffusion coefficient. However, the physical behavior of each realization is very different from that predicted by Fick's deterministic law of diffusion. Instead of each mode being independent of all other modes as in simple (linear) diffusion, the random advection couples all the modes and produces large-scale giant fluctuations in the concentration. These are manifested in a power-law behavior of the spectrum of concentrations, as predicted by linearized fluctuating hydrodynamics and observed in recent experiments [4–6].

Here we studied coarse-graining based on a continuum rather than a discrete microscopic model of diffusion. An alternative approach to coarse-graining of diffusion is to consider purely discrete models in which the coarse-grained variables are not smothed fields, as we have done here, but rather, a collection of discrete variables associated with coarse-graining volumes (cells) of length $\delta \gg \sigma$ [28, 55]. The accuracy of such finite-dimensional truncations can, in principle, be evaluated by comparing them to particle simulations. As an alternative, one can start from the more tractable continuum model (5) and think of finite-dimensional truncations as discretizations of (25). In the end, our numerical observations suggest that at scales much larger than the molecular the behavior of all models is similar, and can be described by a combination of bare diffusion and advection by a thermally fluctuating velocity field. Understanding this equivalence mathematically is a challenge common to all dynamical coarse-graining endeavors.

In typical experiments, such as FRAP measurements of diffusion coefficients, one observes the concentration spatially-coarse grained at scales much larger than the molecular scale. We discussed how to perform such spatial coarse-graining for the conditional ensemble average over only the unresolved velocity fluctuations. This conditional mean shows true dissipation in the form of a renormalized diffusion coefficient, a remnant of the eliminated degrees of freedom. We observed numerically that the equation for the conditional ensemble average is a good approximation (closure) to the dynamics of individual realizations of the spatially coarse-grained concentration. This means that, even in the absence of bare diffusion, the coarse-grained concentration shows dissipative behavior, as we confirmed using Lagrangian numerical simulations. The renormalized diffusion coefficient in the coarse-grained equation is nonzero even in the absence of bare diffusion, and, in fact, one can set $\chi_0 = 0$ without affecting the behavior of the concentration field at mesoscopic scales. The renormalized diffusion coefficient is then controlled by the molecular scale σ only, in agreement with Stokes-Einstein's formula. Contrary to the standard renormalization theory [7, 12] which accounts for the contribution of thermal fluctuations as a perturbation (correction) to the bare (molecular) diffusion coefficient, in our model diffusion arises *entirely* due to the velocity fluctuations and it is not necessary to include an *ad hoc* bare diffusion term.

In the limit of infinite coarse-graining length scale, at least in three dimensions, one expects to obtain the usual Fick's law of diffusion. That is, we expect that at macroscopic scales one recovers the deterministic diffusion equation (11) not just for the ensemble mean but also (as a law of large numbers) for each instance (realization) of the mixing process. Understanding the precise relationship between the macroscopic and microscopic dynamics is a challenge even for much simpler models of diffusion such as the case of non-interacting Brownian walkers [56, 57]; it therefore remains an important future challenge to understand the precise relationship between Fick's law, (9) (equivalently, (5)) and (21), in three dimensions. In two dimensions, however, there is no macroscopic limit because the renormalized diffusion coefficient grows logarithmically with system size.

More importantly, in both two and three dimensions the behavior of a diffusive mixing process cannot be described by Fick's law at mesoscopic scales. One must include random advection by the mesoscopic scales of the velocity fluctuations in order to reproduce not just the behavior of the mean but also the giant fluctuations observed in individual realizations (instances). The diffusion renormalization depends sensitively on the spectrum of the velocity fluctuations, which is affected by boundary conditions (confinement) [9, 10, 54]. The traditional Fick's diffusion constant is only meaningful under special conditions which may not in fact be satisfied in many experiments aimed to measure "the" diffusion coefficient. A length scale of observation (coarse-graining) must be attached to the diffusion coefficient value in order to make it a true "material constant" that can be used in a predictive model of diffusive transport [9].

Dismissing the effect of thermal fluctuations as "weak" is easy with hand-waving estimates, but not

easily justified upon an in-depth analysis as we have performed here. We hope that our work will spur interest in designing experiments that carefully examine diffusion at a broad range of length scales. Existing experiments have been able to measure concentration fluctuations across a wide range of lenghtscales transverse to the gradient, but fluctuations are averaged longitudinally over essentially macroscopic scales (thickness of the sample) [4–6]. FRAP experiments routinely look at diffusion at micrometer scales, however, we are not aware of any work that has even attempted to account for the important effect of thermal fluctuations. It is perhaps not surprising that diffusion coefficients in liquids are typically only known to at most a couple of decimal places. The renormalization of the diffusion coefficient by the velocity fluctuations depends on the geometry of the sample and the initial excitation, and on factors such as gravity and surface tension. Giant fluctuations are expected to be more easily observed and measured in thin liquid films due to the quasi-two dimensional geometry [54, 58].

Recently, nonequilibrium fluctuations have been used as a way to measure mass and thermophoretic diffusion coefficients more accurately [59]. Our work is directly relevant to such efforts, especially when combined with numerical methods to solve the resulting stochastic advection-diffusion equations [29, 31]. The simple model we considered here is only applicable to self-diffusion or diffusion of tracers in the dilute regime. Generalizing the model and in particular the mode-elimination procedure to more realistic binary fluid mixtures is an important future research direction. To our knowledge, there have been no studies of the renormalization of diffusion by thermal velocity fluctuations in ternary mixtures. In the future we will consider extensions of our approach to multispecies liquid mixtures. Such extensions are expected to lead to a better understanding of the physics of diffusion in fluid mixtures, including a generalized Stokes-Einstein relation for inter-diffusion coefficients in dilute multispecies solutions.

Appendix

A.   Mode Elimination Procedure

In this appendix we consider the system of equations (1,3,4) in the limit of infinite Schmidt number. For completeness, and because gravity is known to strongly affect giant fluctuations [5, 6, 60, 61] in actual experiments, we include here a buoyancy term in the velocity (momentum) equation. This introduces a coupling of concentration back into the velocity equation. It is convenient to eliminate the incompressibility constraint by using a projection operator formalism to remove the pressure from the fluctuating Navier-Stokes equation,

$$\rho \partial_t \boldsymbol{v} = \boldsymbol{\mathcal{P}} \left[\eta \boldsymbol{\nabla}^2 \boldsymbol{v} + \boldsymbol{\nabla} \cdot \left(\sqrt{2\eta k_B T}\, \boldsymbol{\mathcal{W}} \right) - \beta \rho c\, \boldsymbol{g} \right] \tag{A1}$$

$$\partial_t c = - \boldsymbol{u} \cdot \boldsymbol{\nabla} c + \chi_0 \boldsymbol{\nabla}^2 c + \boldsymbol{\nabla} \cdot \left(\sqrt{2\chi_0 c}\, \boldsymbol{\mathcal{W}}_c \right). \tag{A2}$$

Here $\boldsymbol{u} = \boldsymbol{\sigma} \star \boldsymbol{v}$ is the mollified version of $\boldsymbol{v}$ defined in (3), β is the solutal expansion coefficient (assumed constant), and $\boldsymbol{g}$ is the graviational acceleration; $\boldsymbol{\mathcal{P}}$ is the orthogonal projection onto the space of divergence-free velocity fields, $\boldsymbol{\mathcal{P}} = \boldsymbol{I} - \boldsymbol{\mathcal{G}} \left(\boldsymbol{\mathcal{D}} \boldsymbol{\mathcal{G}} \right)^{-1} \boldsymbol{\mathcal{D}}$ in real space, where $\boldsymbol{\mathcal{D}} \equiv \boldsymbol{\nabla}\cdot$ denotes the divergence operator and $\boldsymbol{\mathcal{G}} \equiv \boldsymbol{\nabla}$ the gradient operator, with the appropriate boundary conditions taken into account. With periodic boundaries we can express all operators in Fourier space and $\widehat{\boldsymbol{\mathcal{P}}} = \boldsymbol{I} - k^{-2}(\boldsymbol{k}\boldsymbol{k}^T)$, where $\boldsymbol{k}$ is the wave number. Note that our inclusion of the problematic multiplicative-noise term $\boldsymbol{\nabla} \cdot \left(\sqrt{2\chi_0 c}\, \boldsymbol{\mathcal{W}}_c \right)$ is purely formal, as a precise interpretation of this term is missing. For the purposes of this calculation we simply carry that term through.

In this Appendix, we formally show that there exists a limiting dynamics for c as the bare Schmidt number $\mathrm{Sc}_0 = \eta/ \left(\rho \chi_0 \right) \to \infty$ and $\chi_0 \to 0$ in such a way that

$$\chi_0^2 \mathrm{Sc}_0 \sim \chi_0 \eta = \mathrm{const},$$

which is consistent with the scaling of the diffusion coefficient with viscosity predicted by the Stokes-Einstein

relation (15). To this end, consider a family of equations in which the coefficients are rescaled as

$$\eta \mapsto \epsilon^{-1}\eta, \qquad \chi_0 \mapsto \epsilon\chi_0. \tag{A3}$$

This rescaling preserves the product $\chi_0\eta$ but implies that $\text{Sc}_0 \mapsto \epsilon^{-2}\text{Sc}_0$, so that the rescaled $\text{Sc}_0 \to \infty$ as $\epsilon \to 0$. For $\epsilon = 1$ we get the original dynamics (A1,A2), and as $\epsilon \to 0$ we get the dynamics in the limit of infinite Schmidt number. If the separation of time scales in the original dynamics is sufficiently strong the limiting dynamics $\epsilon \to 0$ is a good proxy for the real dynamics $\epsilon = 1$. This assumption of separation of time scales has to be verified *a posteriori*, after the limiting dynamics is obtained; specifically, the actual dimensionless number of interest is not the bare Sc_0 but rather the effective $\text{Sc} = \eta/(\rho\chi_{\text{eff}}) \to \infty$.

Writing (A1) in terms of the rescaled coefficients (A3) and rescaling time as $t \mapsto \epsilon^{-1}t$, we arrive at the rescaled system

$$\partial_t \breve{\boldsymbol{v}} = \mathcal{P}\left[\epsilon^{-2}\eta\rho^{-1}\boldsymbol{\nabla}^2\breve{\boldsymbol{v}} + \boldsymbol{\nabla}\cdot\left(\sqrt{2\epsilon^{-2}\eta\rho^{-2}\,k_BT}\,\boldsymbol{\mathcal{W}}(t)\right) - \epsilon^{-1}\beta\breve{c}\,\boldsymbol{g}\right] \tag{A4}$$

$$\partial_t \breve{c} = -\epsilon^{-1}\breve{\boldsymbol{u}}\cdot\boldsymbol{\nabla}\breve{c} + \chi_0\boldsymbol{\nabla}^2\breve{c} + \boldsymbol{\nabla}\cdot\left(\sqrt{2\chi_0\breve{c}}\,\boldsymbol{\mathcal{W}}_c(t)\right). \tag{A5}$$

These equations define a Markov process with generator $\boldsymbol{L} = \boldsymbol{L}_0 + \epsilon^{-1}\boldsymbol{L}_1 + \epsilon^{-2}\boldsymbol{L}_2$, where

$$\boldsymbol{L}_0 F = \chi_0\int d\boldsymbol{r}\,\boldsymbol{\nabla}^2 c(\boldsymbol{r})\frac{\delta F}{\delta c(\boldsymbol{r})} + \chi_0\int d\boldsymbol{r}\,c(\boldsymbol{r})\boldsymbol{\nabla}^2\frac{\delta^2 F}{\delta c(\boldsymbol{r})^2}$$

$$\boldsymbol{L}_1 F = -\int d\boldsymbol{r}\,\boldsymbol{u}(\boldsymbol{r})\cdot\boldsymbol{\nabla}c(\boldsymbol{r})\frac{\delta F}{\delta c(\boldsymbol{r})} + \beta\int d\boldsymbol{r}\,\mathcal{P}(c(\boldsymbol{r})\boldsymbol{g})\cdot\frac{\delta F}{\delta\boldsymbol{v}(\boldsymbol{r})} \tag{A6}$$

$$\boldsymbol{L}_2 F = \eta\rho^{-1}\int d\boldsymbol{r}\,\mathcal{P}\boldsymbol{\nabla}^2\boldsymbol{v}\cdot\frac{\delta F}{\delta\boldsymbol{v}(\boldsymbol{r})} + \eta\rho^{-2}k_BT\int d\boldsymbol{r}\mathcal{P}\boldsymbol{\nabla}\boldsymbol{\nabla}:\frac{\delta^2 F}{\delta\boldsymbol{v}(\boldsymbol{r})^2},$$

and $\delta F/\delta c(\boldsymbol{r})$ denotes the functional derivative of the functional $F \equiv F[c, \boldsymbol{v}]$ with respect to the field $c(\boldsymbol{r})$ and similarly for $\delta F/\delta\boldsymbol{v}(\boldsymbol{r})$. Note that the operator $\boldsymbol{L}_2$ is the generator of the so-called virtual fast process, which is nothing more than the equation for the fast (i.e., the fluctuating) velocity component written in its natural time scale $\tau = t/\epsilon^2$,

$$\partial_\tau \tilde{\boldsymbol{v}} = \mathcal{P}\left[\eta\rho^{-1}\boldsymbol{\nabla}^2\tilde{\boldsymbol{v}} + \boldsymbol{\nabla}\cdot\left(\sqrt{2\eta\rho^{-2}\,k_BT}\,\boldsymbol{\mathcal{W}}(\tau)\right)\right]. \tag{A7}$$

This process describes the dynamics of equilibrium fluctuations of velocity in the Stokes regime. The dynamics is time-reversible with respect to a Gaussian Gibbs-Boltzmann equilibrium distribution which, for a periodic system, can be formally written as [30]

$$P_{\text{eq}}(\tilde{\boldsymbol{v}}) = Z^{-1}\exp\left[-\frac{\int d\boldsymbol{r}\,\rho\tilde{v}^2}{2k_BT}\right]\boldsymbol{\delta}\left(\int d\boldsymbol{r}\,\rho\tilde{\boldsymbol{v}}\right)\delta\left(\boldsymbol{\nabla}\cdot\tilde{\boldsymbol{v}}\right). \tag{A8}$$

The mathematical asymptotic expansion techniques we employ follow the procedure introduced in [15, 32, 33] (for a review see also the book [34]). Denote by $(\breve{c}(\boldsymbol{r}, t), \breve{\boldsymbol{v}}(\boldsymbol{r}, t))$ the solution to (A4,A5) for the initial conditions $(\breve{c}(\boldsymbol{r}, 0), \breve{\boldsymbol{v}}(\boldsymbol{r}, 0)) = (c(\boldsymbol{r}), \boldsymbol{v}(\boldsymbol{r}))$ and consider

$$\langle F[\breve{c}(\cdot, t)]\rangle \equiv G[c(\cdot), \boldsymbol{v}(\cdot), t], \tag{A9}$$

where the expectation $\langle\cdot\rangle$ is taken over the realizations of the noise terms $\boldsymbol{\mathcal{W}}(t)$ and $\boldsymbol{\mathcal{W}}_c(t)$. This expectation defines a time-dependent functional G of the initial conditions which satisfies the (functional) backward Kolmogorov equation

$$\partial_t G = \boldsymbol{L}_0 G + \epsilon^{-1}\boldsymbol{L}_1 G + \epsilon^{-2}\boldsymbol{L}_2 G, \qquad G|_{t=0} = F. \tag{A10}$$

We wish to take the limit as $\epsilon \to 0$ of this equation. To this end, formally expand G as

$$G = G_0 + \epsilon G_1 + \epsilon^2 G_2 + \cdots \tag{A11}$$

and insert this expression in (A10), and collect terms of increasing power in ϵ. This gives the hierarchy

$$\boldsymbol{L}_2 G_0 = 0,$$
$$\boldsymbol{L}_2 G_1 = -\boldsymbol{L}_1 G_0,$$
$$\boldsymbol{L}_2 G_2 = \partial_t G_0 - \boldsymbol{L}_0 G_0 - \boldsymbol{L}_1 G_1, \tag{A12}$$
$$\vdots$$

The first equation in (A12) indicates that G_0 is a functional of $c(\boldsymbol{r})$ alone, rather than $c(\boldsymbol{r})$ and $\boldsymbol{v}(\boldsymbol{r})$, i.e.

$$G_0 \equiv G_0[c]. \tag{A13}$$

The second equation in (A12) requires a solvability condition, namely that its right hand side be in the range of the operator $\boldsymbol{L}_2$. Equivalently, the expectation of any term involving $\boldsymbol{v}(\boldsymbol{r})$ in this right hand side with respect to the invariant measure of the virtual fast process $\tilde{\boldsymbol{v}}(\boldsymbol{r}, t)$ given by (A8) must be zero. Denoting this expectation by $\langle f \rangle_{\boldsymbol{v}} = \int f(\tilde{\boldsymbol{v}}) \, P_{\text{eq}}(\tilde{\boldsymbol{v}}) \, \mathcal{D}\tilde{\boldsymbol{v}}$, where the integral is a formal functional integral, the solvability condition can be written as

$$0 = \langle \boldsymbol{L}_1 G_0 \rangle_{\boldsymbol{v}} \equiv - \int d\boldsymbol{r} \langle \boldsymbol{u}(\boldsymbol{r}) \rangle_{\boldsymbol{v}} \cdot \boldsymbol{\nabla} c(\boldsymbol{r}) \frac{\delta G_0}{\delta c(\boldsymbol{r})} \tag{A14}$$

where we used the fact that G_0 is a functional of c alone from (A13). This solvability condition is automatically satisfied since $\langle \boldsymbol{v}(\boldsymbol{r}) \rangle_{\boldsymbol{v}} = 0$. As a result, the second equation in (A12) can be solved in G_1 to obtain

$$G_1 = - \boldsymbol{L}_2^{-1} \boldsymbol{L}_1 G_0 \tag{A15}$$

where $\boldsymbol{L}_2^{-1}$ denotes the pseudo-inverse of $\boldsymbol{L}_2$. The third equation in (A12) also requires a solvability condition, which reads

$$\begin{aligned} \partial_t G_0 &= \langle \boldsymbol{L}_0 G_0 \rangle_{\boldsymbol{v}} + \langle \boldsymbol{L}_1 G_1 \rangle_{\boldsymbol{v}} \\ &= \boldsymbol{L}_0 G_0 - \left\langle \boldsymbol{L}_1 \boldsymbol{L}_2^{-1} \boldsymbol{L}_1 G_0 \right\rangle_{\boldsymbol{v}} \end{aligned} \tag{A16}$$

where we used $\langle \boldsymbol{L}_0 G_0 \rangle_{\boldsymbol{v}} = \boldsymbol{L}_0 G_0$ as well as (A15) to get the second equality.

To write the second term on the right hand side of (A16) explicitly notice that

$$\boldsymbol{L}_1 G_0 = - \int d\boldsymbol{r} \; \boldsymbol{u}(\boldsymbol{r}) \cdot \boldsymbol{\nabla} c(\boldsymbol{r}) \frac{\delta G_0}{\delta c(\boldsymbol{r})} \tag{A17}$$

Since this operator is linear in $\boldsymbol{u}(\boldsymbol{r}) = \boldsymbol{\sigma} \star \boldsymbol{v}(\boldsymbol{r})$, to compute the action of $\boldsymbol{L}_2^{-1}$ on it, we can use

$$\begin{aligned} \boldsymbol{L}_2^{-1} \boldsymbol{u}(\boldsymbol{r}) &= \boldsymbol{L}_2^{-1} \boldsymbol{\sigma} \star \boldsymbol{v}(\boldsymbol{r}) = \boldsymbol{\sigma} \star \boldsymbol{L}_2^{-1} \boldsymbol{v}(\boldsymbol{r}) \\ &= -\boldsymbol{\sigma} \star \int_0^\infty d\tau \, e^{\tau \boldsymbol{L}_2} \boldsymbol{v}(\boldsymbol{r}) = -\boldsymbol{\sigma} \star \int_0^\infty d\tau \, \langle \tilde{\boldsymbol{v}}(\boldsymbol{r}, \tau) \rangle, \end{aligned} \tag{A18}$$

where $\tilde{\boldsymbol{v}}(\boldsymbol{r}, \tau)$ denotes the solution to (A7) for the initial condition $\tilde{\boldsymbol{v}}(\boldsymbol{r}, 0) = \boldsymbol{v}(\boldsymbol{r})$ and the expectation is the same as in (A9). From (A7), this solution can be formally expressed as

$$\begin{aligned} \tilde{\boldsymbol{v}}(\boldsymbol{r}, \tau) &= \exp\left(-\tau \eta \rho^{-1} \boldsymbol{\mathcal{L}}\right) \boldsymbol{v}(\boldsymbol{r}) \\ &+ \int_0^\tau d\tau' \, \exp\left(-(\tau - \tau')\eta\rho^{-1} \boldsymbol{\mathcal{L}}\right) \boldsymbol{\nabla} \cdot \left(\sqrt{2\eta\rho^{-2} k_B T} \, \boldsymbol{\mathcal{W}}(\tau')\right), \end{aligned} \tag{A19}$$

where $\boldsymbol{\mathcal{L}} = -\boldsymbol{\mathcal{P}} \boldsymbol{\nabla}^2$ is the Stokes operator. The second term is linear in $\boldsymbol{\mathcal{W}}$ and therefore has zero average and does not contribute to the expectation in (A18) (i.e., it is a martingale). As a result, combining (A18) and (A19) we conclude that

$$\boldsymbol{L}_2^{-1} \boldsymbol{u}(\boldsymbol{r}) = -\rho\eta^{-1} \left(\boldsymbol{G}_\sigma \star \boldsymbol{v}\right)(\boldsymbol{r}) \equiv -\rho\eta^{-1} \int d\boldsymbol{r}' \, \boldsymbol{G}_\sigma(\boldsymbol{r}, \boldsymbol{r}') \boldsymbol{v}(\boldsymbol{r}') \tag{A20}$$

where $\boldsymbol{G}_\sigma = \boldsymbol{\sigma} \star \boldsymbol{G}$ and $\boldsymbol{G}(\boldsymbol{r}, \boldsymbol{r}')$ is the Green's function for Stokes flow. More explicitly, $\boldsymbol{G}_\sigma \star \boldsymbol{v} \equiv \boldsymbol{\sigma} \star \boldsymbol{\mathcal{L}}^{-1} \boldsymbol{v}$ is a shorthand notation for the smoothed solution of the Stokes equation with unit viscosity: $\boldsymbol{w}_\sigma = \boldsymbol{G}_\sigma \star \boldsymbol{v}$ if $\boldsymbol{w}_\sigma = \boldsymbol{\sigma} \star \boldsymbol{w}$ and $\boldsymbol{w}$ solves

$$\boldsymbol{\nabla} \pi = \boldsymbol{\nabla}^2 \boldsymbol{w} + \boldsymbol{v}, \qquad \boldsymbol{\nabla} \cdot \boldsymbol{w} = 0. \tag{A21}$$

Using (A20) and the obvious identity

$$\frac{\delta c(\boldsymbol{r}')}{\delta c(\boldsymbol{r})} = \delta(\boldsymbol{r} - \boldsymbol{r}'), \tag{A22}$$

we see that the second term on the right hand side of (A16) can be written as

$$
\begin{aligned}
&- \left\langle \boldsymbol{L}_1 \boldsymbol{L}_2^{-1} \boldsymbol{L}_1 G_0 \right\rangle_v \\
&= \rho\eta^{-1} \int d\boldsymbol{r} d\boldsymbol{r}' \, \boldsymbol{\nabla} c(\boldsymbol{r}) \cdot \frac{\delta}{\delta c(\boldsymbol{r})} \left(\left\langle (\boldsymbol{\sigma} \star \boldsymbol{v}(\boldsymbol{r})) \otimes (\boldsymbol{G}_\sigma \star \boldsymbol{v}(\boldsymbol{r}')) \right\rangle_v \cdot \boldsymbol{\nabla}' c(\boldsymbol{r}') \frac{\delta G_0}{\delta c(\boldsymbol{r}')} \right) \\
&\quad - \beta\rho\eta^{-1} \int d\boldsymbol{r} d\boldsymbol{r}' \, \boldsymbol{\mathcal{P}}(c(\boldsymbol{r})\boldsymbol{g}) \cdot \left\langle \frac{\delta}{\delta \boldsymbol{v}(\boldsymbol{r})} (\boldsymbol{G}_\sigma \star \boldsymbol{v}(\boldsymbol{r}')) \right\rangle_v \cdot \boldsymbol{\nabla}' c(\boldsymbol{r}') \frac{\delta G_0}{\delta c(\boldsymbol{r}')} \\
&= \rho\eta^{-1} \int d\boldsymbol{r} d\boldsymbol{r}' \, \boldsymbol{\nabla} c(\boldsymbol{r}) \cdot \left\langle (\boldsymbol{\sigma} \star \boldsymbol{v}(\boldsymbol{r})) \otimes (\boldsymbol{G}_\sigma \star \boldsymbol{v}(\boldsymbol{r}')) \right\rangle_v \cdot \left(\boldsymbol{\nabla}' c(\boldsymbol{r}') \frac{\delta^2 G_0}{\delta c(\boldsymbol{r}) \delta c(\boldsymbol{r}')} - \boldsymbol{\nabla}' \delta(\boldsymbol{r}' - \boldsymbol{r}) \frac{\delta G_0}{\delta c(\boldsymbol{r}')} \right) \\
&\quad - \beta\rho\eta^{-1} \int d\boldsymbol{r} d\boldsymbol{r}' \, \boldsymbol{\mathcal{P}}(c(\boldsymbol{r})\boldsymbol{g}) \cdot \left\langle \frac{\delta}{\delta \boldsymbol{v}(\boldsymbol{r})} (\boldsymbol{G}_\sigma \star \boldsymbol{v}(\boldsymbol{r}')) \right\rangle_v \cdot \boldsymbol{\nabla}' c(\boldsymbol{r}') \frac{\delta G_0}{\delta c(\boldsymbol{r}')},
\end{aligned}
\tag{A23}
$$

where $\boldsymbol{\nabla}'$ denotes the gradient operator with respect to $\boldsymbol{r}'$. The first equality will be useful to write the limiting equation for c in Stratonovich's form, and the second one in Ito's form.

To proceed further we need to explicitly perform the averages over the equilibrium distribution of the fast virtual process,

$$
\rho\eta^{-1} \left\langle (\boldsymbol{\sigma} \star \boldsymbol{v}(\boldsymbol{r})) \otimes (\boldsymbol{G}_\sigma \star \boldsymbol{v}(\boldsymbol{r}')) \right\rangle_v = \tfrac{1}{2} \boldsymbol{\mathcal{R}}(\boldsymbol{r}, \boldsymbol{r}'),
\tag{A24}
$$

where $\boldsymbol{\mathcal{R}}(\boldsymbol{r}, \boldsymbol{r}')$ is the tensor defined in (7), and (using $\delta\boldsymbol{v}(\boldsymbol{r}')/\delta\boldsymbol{v}(\boldsymbol{r}) = \boldsymbol{\delta}(\boldsymbol{r} - \boldsymbol{r}')$)

$$
\begin{aligned}
&\int d\boldsymbol{r} \, \boldsymbol{\mathcal{P}}(c(\boldsymbol{r})\boldsymbol{g}) \cdot \left\langle \frac{\delta}{\delta \boldsymbol{v}(\boldsymbol{r})} (\boldsymbol{G}_\sigma \star \boldsymbol{v}(\boldsymbol{r}')) \right\rangle_v \\
&= \int d\boldsymbol{r} d\boldsymbol{r}'' \, \boldsymbol{\mathcal{P}}(c(\boldsymbol{r})\boldsymbol{g}) \cdot \left\langle \frac{\delta}{\delta \boldsymbol{v}(\boldsymbol{r})} (\boldsymbol{G}_\sigma(\boldsymbol{r}', \boldsymbol{r}'')\boldsymbol{v}(\boldsymbol{r}'')) \right\rangle_v \\
&= \int d\boldsymbol{r} d\boldsymbol{r}'' \, \boldsymbol{\mathcal{P}}(c(\boldsymbol{r})\boldsymbol{g}) \, (\boldsymbol{G}_\sigma(\boldsymbol{r}', \boldsymbol{r}'')\boldsymbol{\delta}(\boldsymbol{r} - \boldsymbol{r}'')) \\
&= \int d\boldsymbol{r}'' \, \boldsymbol{G}_\sigma(\boldsymbol{r}', \boldsymbol{r}'')\boldsymbol{\mathcal{P}}(c(\boldsymbol{r}'')\boldsymbol{g}) \\
&= (\boldsymbol{G}_\sigma \star \boldsymbol{\mathcal{P}}c)(\boldsymbol{r}') \, \boldsymbol{g}.
\end{aligned}
\tag{A25}
$$

Inserting (A24) and (A25) in (A23), performing an integration by part and using the property that $\boldsymbol{\nabla} \cdot \boldsymbol{\mathcal{R}}(\boldsymbol{r}, \boldsymbol{r}') = 0$ (which follows from $\boldsymbol{\nabla} \cdot \boldsymbol{u} = 0$) and $\boldsymbol{G}_\sigma \star \boldsymbol{\mathcal{P}} = \boldsymbol{G}_\sigma$ (which follows from $\boldsymbol{\mathcal{P}}\boldsymbol{\mathcal{L}}^{-1} = \boldsymbol{\mathcal{L}}^{-1}\boldsymbol{\mathcal{P}} = \boldsymbol{\mathcal{L}}^{-1}$) we finally obtain

$$
\begin{aligned}
&- \left\langle \boldsymbol{L}_1 \boldsymbol{L}_2^{-1} \boldsymbol{L}_1 G_0 \right\rangle_v \\
&= \tfrac{1}{2} \int d\boldsymbol{r} d\boldsymbol{r}' \, \boldsymbol{\nabla} c(\boldsymbol{r}) \cdot \frac{\delta}{\delta c(\boldsymbol{r})} \left(\boldsymbol{\mathcal{R}}(\boldsymbol{r}, \boldsymbol{r}') \cdot \boldsymbol{\nabla}' c(\boldsymbol{r}') \frac{\delta G_0}{\delta c(\boldsymbol{r}')} \right) \\
&\quad + \beta\rho\eta^{-1} \int d\boldsymbol{r} \, (\boldsymbol{G}_\sigma \star c)(\boldsymbol{r})\boldsymbol{g} \cdot \boldsymbol{\nabla} c(\boldsymbol{r}) \frac{\delta G_0}{\delta c(\boldsymbol{r})} \\
&= \tfrac{1}{2} \int d\boldsymbol{r} d\boldsymbol{r}' \, \boldsymbol{\nabla} c(\boldsymbol{r}) \cdot \boldsymbol{\mathcal{R}}(\boldsymbol{r}, \boldsymbol{r}') \cdot \boldsymbol{\nabla}' c(\boldsymbol{r}') \frac{\delta^2 G_0}{\delta c(\boldsymbol{r}) \delta c(\boldsymbol{r}')} \\
&\quad + \int d\boldsymbol{r} \, \boldsymbol{\nabla} \cdot (\boldsymbol{\chi}(\boldsymbol{r}) \boldsymbol{\nabla} c(\boldsymbol{r})) \frac{\delta G_0}{\delta c(\boldsymbol{r})} \\
&\quad + \beta\rho\eta^{-1} \int d\boldsymbol{r} \, (\boldsymbol{G}_\sigma \star c)(\boldsymbol{r})\boldsymbol{g} \cdot \boldsymbol{\nabla} c(\boldsymbol{r}) \frac{\delta G_0}{\delta c(\boldsymbol{r})},
\end{aligned}
\tag{A26}
$$

where we recall $\boldsymbol{\chi}(\boldsymbol{r}) = \tfrac{1}{2} \boldsymbol{\mathcal{R}}(\boldsymbol{r}, \boldsymbol{r})$.

Inserting (A26) in (A16) gives the explicit form of the limiting equation for $G_0 = \lim_{\epsilon \to 0} G$. This equation is a backward Kolmogorov equation from which the limiting stochastic differential equation for c as $\epsilon \to 0$ can be read. The second-order functional derivative (with respect to $c(\boldsymbol{r})$) written as in the first form of the right hand side of (A26) gives this equation in Stratonovich's interpretation, while the

second form of the right hand side of (A26) gives it in Ito's interpretation:

$$
\begin{aligned}
dc = & -\sum_k \boldsymbol{\phi}_k \cdot \boldsymbol{\nabla} c \circ d\mathcal{B}_k \\
& + \chi_0 \boldsymbol{\nabla}^2 c \, dt + \boldsymbol{\nabla} \cdot \left(\sqrt{2\chi_0 c} \, d\boldsymbol{\mathcal{B}}_c \right) \\
& + \beta \rho \eta^{-1} \left(\boldsymbol{G}_\sigma \star c \right) \boldsymbol{g} \cdot \boldsymbol{\nabla} c \, dt \\
= & -\sum_k \boldsymbol{\phi}_k \cdot \boldsymbol{\nabla} c \, d\mathcal{B}_k + \boldsymbol{\nabla} \cdot \left(\boldsymbol{\chi} \boldsymbol{\nabla} c \right) dt \\
& + \chi_0 \boldsymbol{\nabla}^2 c \, dt + \boldsymbol{\nabla} \cdot \left(\sqrt{2\chi_0 c} \, d\boldsymbol{\mathcal{B}}_c \right) \\
& + \beta \rho \eta^{-1} \left(\boldsymbol{G}_\sigma \star c \right) \boldsymbol{g} \cdot \boldsymbol{\nabla} c \, dt
\end{aligned}
\tag{A27}
$$

where $\boldsymbol{\mathcal{B}}_c(\boldsymbol{r}, t)$ is the Brownian sheet process such that we formally have $d\boldsymbol{\mathcal{B}}_c/dt = \boldsymbol{\mathcal{W}}_c$. Note that the derivation above, while formal, leaves no ambiguity in terms of the interpretation of the first term at the right hand sides of (A27).

If we set $\boldsymbol{g} = 0$ in this equation, (A27) reduces to (5) and (9). Also note that the gravity does not affect the effective diffusion coefficient in the limit of infinite Schmidt number, as it may for finite Schmidt numbers [8]. However, the spectrum of the fluctuations in concentration at small wavenumbers is strongly affected by buoyancy effects, and (A27) is the nonlinear generalization of the existing linearized fluctuating hydrodynamic theory for this effect [3, 5, 6, 60, 61]. Note that because (A27) is nonlinear, it is no longer possible to take expectation values and write a closed equation for ensemble averages, as it was in the purely linear case.

B. Multiscale Integrators

In this Appendix we describe the multiscale algorithms [62, 63] used to numerically solve the limiting Eulerian (5) and Lagrangian (16) equations. These methods rely on being able to solve the steady Stokes equations with random forcing, more precisely, to generate a random velocity field $\boldsymbol{w}(\boldsymbol{r})$ with spatial covariance

$$
\langle \boldsymbol{w}(\boldsymbol{r}_1) \otimes \boldsymbol{w}(\boldsymbol{r}_2) \rangle = \frac{2k_B T}{\eta} \int \boldsymbol{\sigma}(\boldsymbol{r}_1, \boldsymbol{r}') \boldsymbol{G}(\boldsymbol{r}', \boldsymbol{r}'') \boldsymbol{\sigma}^T(\boldsymbol{r}_2, \boldsymbol{r}'') \, d\boldsymbol{r}' d\boldsymbol{r}''.
$$

For the simulations described here we rely on periodic boundary conditions, which means that the Fourier basis diagonalizes the Stokes operator and therefore one can use the Fast Fourier Transform (FFT) to efficiently solve the steady Stokes equations. This has helped us to implement both the Eulerian and the Lagrangian algorithm on Graphics Processing Units (GPUs), which has enabled simulations with as many as 16 million degrees of freedom. While both algorithms and our codes work in either two or three dimensions, in order to be able to study power law behavior over many decades we focus in this work on two dimensional systems (for $d = 2$ we use up to 2048^2 grid cells or wave-indices, but for $d = 3$ we are presently limited to at most 256^3 grids due to memory requirements).

In principle one can use either the Ito or Stratonovich forms of the limiting dynamics. The only difference is in the temporal integrator, namely, Ito equations can be integrated with the Euler-Maruyama (one-step) scheme, while Stratonovich equations require the Euler-Heun (predictor-corrector) scheme [64]. Here we use the Stratonovich form of the equations because this ensures discrete fluctuation-dissipation balance between the random advection (fluctuation) and the effective diffusion (dissipation). For periodic boundaries, the Ito drift term $[\partial_{\boldsymbol{q}} \cdot \boldsymbol{\chi}(\boldsymbol{q})] \, dt$ in the Lagrangian equation (16) vanishes, and there is no difference between the different stochastic interpretations.

1. Eulerian Algorithm

For completeness, we include a gravitational buoyancy term in the velocity equation and present an algorithm for solving the limiting equation (A27), which includes the effect of gravity. Additional background on the types of spatio-temporal integrators used can be found in previous works by some of us [29–31, 65]; here we only sketch the basic features. We do not include the term $\boldsymbol{\nabla} \cdot \left(\sqrt{2\chi_0 c} \, \boldsymbol{\mathcal{W}}_c \right)$ since properly discretizing this multiplicative noise is nontrivial, and largely irrelevant when studying nonequilibrium fluctuations.

The overdamped Eulerian dynamics can be efficiently simulated using the following Euler-Heun predictor-corrector temporal algorithm with time step size Δt, which updates the concentration from time step n to time step $n + 1$ (denoted here by superscript):

1. Generate a random advection velocity by solving the steady Stokes equation with random forcing,

$$\boldsymbol{\nabla}\pi^n = \eta\left(\boldsymbol{\nabla}^2\boldsymbol{v}^n\right) + \boldsymbol{\nabla}\cdot\left(\sqrt{\frac{2\eta\,k_BT}{\Delta t\Delta V}}\,\boldsymbol{W}^n\right) - \rho\beta c^n\boldsymbol{g}$$

$$\boldsymbol{\nabla}\cdot\boldsymbol{v}^n = 0,$$

and compute $\boldsymbol{u}^n = \boldsymbol{\sigma}\star\boldsymbol{v}^n$ by filtering. Here $\boldsymbol{W}^n$ are a collection of Gaussian random variates generated independently at each time step, and ΔV is the volume of each grid cell.

2. Do a predictor step for (5) by solving for $\tilde{c}^{n+1}$,

$$\frac{\tilde{c}^{n+1} - c^n}{\Delta t} = -\boldsymbol{u}^n\cdot\boldsymbol{\nabla}c^n + \chi_0\boldsymbol{\nabla}^2\left(\frac{c^n + \tilde{c}^{n+1}}{2}\right).$$

3. If gravity is zero, set $\boldsymbol{u}^{n+\frac{1}{2}} = \boldsymbol{u}^n$, otherwise, solve the steady Stokes equation

$$\boldsymbol{\nabla}\pi^{n+\frac{1}{2}} = \eta\left(\boldsymbol{\nabla}^2\boldsymbol{v}^{n+\frac{1}{2}}\right) + \boldsymbol{\nabla}\cdot\left(\sqrt{\frac{2\eta\,k_BT}{\Delta t\Delta V}}\,\boldsymbol{W}^n\right) - \rho\beta\left(\frac{c^n + \tilde{c}^{n+1}}{2}\right)\boldsymbol{g}$$

$$\boldsymbol{\nabla}\cdot\boldsymbol{v}^{n+\frac{1}{2}} = 0,$$

and compute $\boldsymbol{u}^{n+\frac{1}{2}} = \boldsymbol{\sigma}\star\boldsymbol{v}^{n+\frac{1}{2}}$. Note that the same random stress is used here as in the predictor.

4. Take a corrector step for concentration to compute c^{n+1},

$$\frac{c^{n+1} - c^n}{\Delta t} = -\boldsymbol{u}^{n+\frac{1}{2}}\cdot\boldsymbol{\nabla}\left(\frac{c^n + \tilde{c}^{n+1}}{2}\right) + \chi_0\boldsymbol{\nabla}^2\left(\frac{c^n + c^{n+1}}{2}\right).$$

This scheme can be shown to be a weakly first-order accurate temporal integrator for (5); it is a weakly second-order method for the linearized equations (21) with gravity included [30]. Note that advection is treated explicitly. The key to obtaining the correct diffusion enhancement is the fact that the average of c^n and $\tilde{c}^{n+1}$ is used to evaluate the advective fluxes in the corrector step. The bare diffusive fluxes can be obtained via any consistent temporal discretization; here we use the Crank-Nicolson or implicit midpoint rule, but an explicit midpoint rule (as used for the advective fluxes) can also be used since the main stability limitation on the time step comes from the advective Courant number.

We discretize the continuum equations in space using a staggered finite-volume fluctuating hydrodynamics solver [29] and use an iterative Krylov linear solver [65, 66] to solve the steady Stokes equations. In this Eulerian algorithm the difficulty is in discretizing advection, as is well-known from turbulence modeling. Because of the transfer of power from the coarse to the fine scales, advection creates fine-scale features in the solution that cannot be represented on the fixed Eulerian grid. This leads to well-known Gibbs instability, and requires introducing some form of dissipation at the larger wavenumbers. If there is sufficient bare diffusion present to smooth the solution at the scale of the grid, then one can use a strictly non-dissipative discrete advection operator [29]. This strictly non-dissipative centered advection maintain discrete fluctuation-dissipation balance [30], and for this reason we have used it for the simulations reported here. If there is insufficient bare diffusion (in particular, if $\chi_0 = 0$) this approach to handling advection fails and one must introduce some form of *artificial dissipation* in the discrete advection procedure. In the future we will explore more sophisticated minimally-dissipative semi-Lagrangian advection schemes [67, 68] to handle the case of no bare diffusion.

The filtering of the discrete random velocity field $\boldsymbol{v}^n$ required to generate $\boldsymbol{u}^n$ can be done in one of several ways. The first approach, which we have employed in several prior works on fluctuating hydrodynamics [9, 29, 31, 69], is to not perform any filtering. This approach was used when preparing Figs. 1 and 2 and 3. In this case the filtering comes from the truncation of the fluctuating fields on the scale of the grid, that is, $\sigma \approx \Delta x$, where Δx is the grid spacing. In this case, it is possible to explicitly compute the diffusion enhancement for the spatially-discretized equations by a discrete analog of (13). This tedious technical calculation will not be presented here for brevity, and we only quote the result in two dimensions. We obtain that the effective diffusion coefficient for the average concentration in the discrete setting is

$$\chi_{\text{eff}}^{2D} \approx \chi_0 + \frac{k_BT}{4\pi\eta}\ln\frac{L}{\alpha\Delta x}, \tag{B1}$$

where $L \gg \Delta x$ is the length of the square periodic cell (note that for non-square unit cells the diffusion enhancement is not isotropic). Here the coefficient $\alpha = 1.2$ was estimated by computing the inverse of the

discrete Stokes operator numerically. The formula (B1) is the discrete equivalent of (15). In three dimensions,

$$\chi_{\text{eff}}^{3D} \approx \chi_0 + \frac{k_B T}{\eta \alpha \Delta x}, \tag{B2}$$

where the coefficient α can be obtained numerically.

An alternative approach to filtering of the velocity was used when preparing Fig. 4. Namely, in order to directly compare to the Lagrangian algorithm described next, we convolved the discrete advection velocity with an isotropic Gaussian filter using a multiplication in Fourier space. In this case the width (standard deviation) of the Gaussian filter σ needs to be substantially larger than the grid spacing Δx, for example, $\sigma \gtrsim 6\Delta x$, in order to obtain a discrete velocity field that is smooth on the scale of the grid. In such over-resolved simulations one is essentially solving the continuum equations to a very good approximation. Note, however, that the resulting algorithm is not efficient because of the large grid sizes required to resolve the continuum fields with the grid. In practice, if additional filtering of the discrete velocity field is desired, it is much more efficient to perform local partial filtering of the random velocity field using local averaging over two or three neighboring grid cells, as described in the Appendix of Ref. [31]. Such filtering would change the coefficient α in (B1,B2) but not affect the form of the discrete Stokes-Einstein relation.

In order to provide a rough estimate of the relative efficiency of simulating the overdamped dynamics (5) versus simulating the original dynamics (1,4), let us compare the typical time step size for the Eulerian algorithm developed above with the method developed in Ref. [29]. Both methods use an FFT-based implicit fluid solver, which dominates the computational cost, so the cost per time step is similar in the two algorithms. Resolving the inertial fluid dynamics requires a time step on the order of $\Delta t_\nu \sim \Delta x^2 / \nu$, the time it takes for momentum to diffuse across one grid cell. The algorithm summarized above is limited in time step size primarily by the advective Courant number $v\Delta t / \Delta x < 1$, where v is a typical magnitude of the advective velocity obtained by solving the steady Stokes equations with random forcing. We can estimate v by noting that it is the fictitious or effective velocity of a particle diffusing with coefficient χ, $v \sim \sqrt{\chi \Delta t}/\Delta t \sim \sqrt{\chi/\Delta t}$. This gives a time step limit $\Delta t \sim (\Delta x^2/\chi) = \text{Sc}\,\Delta t_\nu$, which is nothing more than the time it takes a tracer to diffuse across a grid cell. This shows that simulating the limiting dynamics is $O\,(\text{Sc})$ times faster than the original dynamics.

2. Lagrangian Algorithm

In the absence of bare dissipation, a faithful discretization of the overdamped equations must resort to a Lagrangian discretization of advection. Here we present an algorithm that solves the limiting Lagrangian equation (16) with all truncation errors strictly controlled to be within numerical roundoff (more precisely, to twelve decimal places when using double-precision arithmetic) and *without* artificial dissipation. Such high numerical accuracy is possible by using a spectral representation of the random flow and the non-uniform fast Fourier transform [51]. Note however that the Lagrangian algorithm is limited in efficiency by the number of tracers required to represent the finest scales, which grows with time, as shown in Fig. 5. For finite collection of tracers, e.g., a finite number of colloids in a periodic box, the Lagrangian algorithm below can be seen as an alternative to more standard Brownian/Stokesian Dynamics that naturally accounts for the effects of confinement [70]. Notably, the algorithm below scales perfectly *linearly* in the number of particles. This has enabled us to do simulations with several million particles. Note that we do not include the effect of gravity (buoyancy) in the Lagrangian algorithm.

The random velocity is smoothed by convolution with an isotropic Gaussian filter $\boldsymbol{\sigma}$, which can be performed as multiplication in Fourier space. The tracer Lagrangian dynamics (16) can be efficiently simulated using the following Lagrangian algorithm with time step size Δt, which updates the tracer positions from time step n to time step $n + 1$ (denoted here by superscript):

1. Generate a random advection velocity by solving the steady Stokes equations with random forcing in the Fourier domain

$$i\boldsymbol{k}\hat{\pi}_{\boldsymbol{k}}^{n+\frac{1}{2}} = -\eta k^2 \hat{\boldsymbol{v}}_{\boldsymbol{k}}^n + \sqrt{\frac{2\eta\,k_B T}{\Delta t}}\,i\boldsymbol{k}\cdot\widehat{\boldsymbol{W}}_{\boldsymbol{k}}^n$$

$$\boldsymbol{k}\cdot\hat{\boldsymbol{v}}_{\boldsymbol{k}}^n = 0,$$

using a grid of N^d wave-indices $\boldsymbol{k}$ consistent with the periodicity. Note that different wave-indices decouple in the Fourier basis and the above procedure requires only solving a linear system of d equations for every wavenumber.

2. Filter the velocity with a Gaussian filter (in Fourier space),

$$\hat{\boldsymbol{w}}_{\boldsymbol{k}}^n = \hat{\boldsymbol{\sigma}}_{\boldsymbol{k}}\hat{\boldsymbol{v}}_{\boldsymbol{k}}^n.$$

Note the Fourier transform $\hat{\boldsymbol{\sigma}}$ of a Gaussian filter $\boldsymbol{\sigma}$ with standard deviation σ is also a Gaussian with standard deviation σ^{-1}.

3. Use the non-uniform FFT [51] to evaluate the velocity at the locations of the tracers, $\boldsymbol{u}^n = \boldsymbol{w}^n(\boldsymbol{q}^n)$.

4. Move the tracers using a forward Euler-Maruyama step,
$$\tilde{\boldsymbol{q}}^{n+1} = \boldsymbol{q}^n + \boldsymbol{u}^n \Delta t + \sqrt{2\chi_0 \Delta t}\, \boldsymbol{W}_{\boldsymbol{q}}^n,$$
where $\boldsymbol{W}_{\boldsymbol{q}}^n$ are i.i.d. standard Gaussian variates generated independently for each particle at each time step.

5. For periodic domains there is no difference between different stochastic interpretations of the Lagrangian equations, and one can set $\boldsymbol{q}^{n+1} = \tilde{\boldsymbol{q}}^{n+1}$. For non-periodic domains, one has to perform a corrector step,
$$\boldsymbol{q}^{n+1} = \boldsymbol{q}^n + \left(\boldsymbol{u}^n + \tilde{\boldsymbol{u}}^{n+1}\right)\frac{\Delta t}{2} + \sqrt{2\chi_0 \Delta t}\, \boldsymbol{W}_{\boldsymbol{q}}^n,$$
where $\tilde{\boldsymbol{u}}^{n+1} = \boldsymbol{w}^n\left(\tilde{\boldsymbol{q}}^{n+1}\right)$.

The key to obtaining near roundoff accuracy is the choice of the number of Fourier modes used to represent the fluctuating velocity field. Assume that the Gaussian filter $\hat{\boldsymbol{\sigma}}$ decays to roundoff tolerance above a wavenumber $k_0 \approx 3\sigma$. This means that the Stokes equations only need to be solved for wavenumbers smaller than k_0. In order to also be able to perform the non-uniform FFT with twelve digits of accuracy using a uniform FFT as in the algorithm we use [51], it is necessary to include redundant modes and set the cutoff wavenumber to $2k_0$. This determines the size of the grid used to perform the forward and inverse FFT transforms to $N > 2k_0 L/\pi$, which can be a large number but the algorithm is easily parallelized on GPUs.

For a sufficiently small time step $\Delta t \ll \sigma^2/\chi_{\text{eff}}$, the Lagrangian algorithm described here solves the continuum equations to high accuracy, and the diffusion enhancement can be determined from the continuum formula (13) in Fourier space. For a Gaussian filter of standard deviation σ in two dimensions the relation (B1) with $\Delta x = \sigma$ holds, where we numerically estimate the coefficient $\alpha \approx 5.5$.

---

* Electronic address: donev@courant.nyu.edu
† Electronic address: eve2@courant.nyu.edu

[1] J. R. Dorfman, T. R. Kirkpatrick, and J. V. Sengers. Generic long-range correlations in molecular fluids. *Annual Review of Physical Chemistry*, 45(1):213–239, 1994.

[2] D. Brogioli, A. Vailati, and M. Giglio. Universal behavior of nonequilibrium fluctuations in free diffusion processes. *Phys. Rev. E*, 61:R1–R4, 2000.

[3] J. M. O. De Zarate and J. V. Sengers. *Hydrodynamic fluctuations in fluids and fluid mixtures*. Elsevier Science Ltd, 2006.

[4] A. Vailati and M. Giglio. Giant fluctuations in a free diffusion process. *Nature*, 390(6657):262–265, 1997.

[5] F. Croccolo, D. Brogioli, A. Vailati, M. Giglio, and D. S. Cannell. Nondiffusive decay of gradient-driven fluctuations in a free-diffusion process. *Phys. Rev. E*, 76(4):041112, 2007.

[6] A. Vailati, R. Cerbino, S. Mazzoni, C. J. Takacs, D. S. Cannell, and M. Giglio. Fractal fronts of diffusion in microgravity. *Nature Communications*, 2:290, 2011.

[7] D. Bedeaux and P. Mazur. Renormalization of the diffusion coefficient in a fluctuating fluid I. *Physica*, 73:431–458, 1974.

[8] D. Brogioli and A. Vailati. Diffusive mass transfer by nonequilibrium fluctuations: Fick's law revisited. *Phys. Rev. E*, 63(1):12105, 2000.

[9] A. Donev, A. L. Garcia, Anton de la Fuente, and J. B. Bell. Enhancement of Diffusive Transport by Nonequilibrium Thermal Fluctuations. *J. of Statistical Mechanics: Theory and Experiment*, 2011:P06014, 2011.

[10] F. Detcheverry and L. Bocquet. Thermal fluctuations in nanofluidic transport. *Phys. Rev. Lett.*, 109:024501, 2012.

[11] A. J. Majda and P. R. Kramer. Simplified models for turbulent diffusion: theory, numerical modelling, and physical phenomena. *Physics Reports*, 314(4-5):237–574, 1999.

[12] P. Mazur and D. Bedeaux. Renormalization of the diffusion coefficient in a fluctuating fluid II. *Physica*, 75:79–99, 1974.

[13] D. Bedeaux and P. Mazur. Renormalization of the diffusion coefficient in a fluctuating fluid III. Diffusion of a Brownian particle with finite size. *Physica A Statistical Mechanics and its Applications*, 80:189–202, 1975.

[14] C. W. Gardiner and M. L. Steyn-Ross. Adiabatic elimination in stochastic systems. I-III. *Phys. Rev. A*, 29:2814–2844, 1984.

[15] G. C. Papanicolaou. Some probabilistic problems and methods in singular perturbations. *Rocky Mountain J. Math*, 6(4):653–674, 1976.

[16] H Frusawa and R Hayakawa. On the controversy over the stochastic density functional equations. *Journal of Physics A: Mathematical and General*, 33(15):L155, 2000.

[17] Pep Español and Hartmut Löwen. Derivation of dynamical density functional theory using the projection operator technique. *J. Chem. Phys.*, 131:244101, 2009.

[18] Andrew J Archer and Markus Rauscher. Dynamical density functional theory for interacting brownian particles: stochastic or deterministic? *Journal of Physics A: Mathematical and General*, 37(40):9325, 2004.

[19] David S Dean. Langevin equation for the density of a system of interacting langevin processes. *Journal of Physics A: Mathematical and General*, 29(24):L613, 1996.

[20] Umberto Marini Bettolo Marconi and Pedro Tarazona. Dynamic density functional theory of fluids. *The Journal of Chemical Physics*, 110(16):8032–8044, 1999.

[21] M Rex and H Löwen. Dynamical density functional theory with hydrodynamic interactions and colloids in unstable traps. *Phys. Rev. Lett.*, 101(14):148302, 2008.

[22] Benjamin D. Goddard, Andreas Nold, Nikos Savva, Grigorios A. Pavliotis, and Serafim Kalliadasis. General dynamical density functional theory for classical fluids. *Phys. Rev. Lett.*, 109:120603, 2012.

[23] H. C. Öttinger. *Beyond equilibrium thermodynamics*. Wiley Online Library, 2005.

[24] J. T. Hynes, R. Kapral, and M. Weinberg. Molecular theory of translational diffusion: Microscopic generalization of the normal velocity boundary condition. *J. Chem. Phys.*, 70(3):1456, February 1979.

[25] C. Foias, D. D Holm, and E. S Titi. The Navier–Stokes-alpha model of fluid turbulence. *Physica D: Nonlinear Phenomena*, 152:505–519, 2001.

[26] M. van Reeuwijk, H. J. J. Jonker, and K. Hanjalic̀. Incompressibility of the Leray-α model for wall-bounded flows. *Physics of Fluids*, 18(1):018103, January 2006.

[27] A. Donev and E. Vanden-Eijnden. Dynamic Density Functional Theory with hydrodynamic interactions and fluctuations. In preparation, 2014.

[28] P. Español and I. Zúñiga. On the definition of discrete hydrodynamic variables. *J. Chem. Phys*, 131:164106, 2009.

[29] F. Balboa Usabiaga, J. B. Bell, R. Delgado-Buscalioni, A. Donev, T. G. Fai, B. E. Griffith, and C. S. Peskin. Staggered Schemes for Fluctuating Hydrodynamics. *SIAM J. Multiscale Modeling and Simulation*, 10(4):1369–1408, 2012.

[30] S. Delong, B. E. Griffith, E. Vanden-Eijnden, and A. Donev. Temporal Integrators for Fluctuating Hydrodynamics. *Phys. Rev. E*, 87(3):033302, 2013.

[31] A. Donev, A. J. Nonaka, Y. Sun, T. G. Fai, A. L. Garcia, and J. B. Bell. Low Mach Number Fluctuating Hydrodynamics of Diffusively Mixing Fluids. To appear in CAMCOS, ArXiv preprint 1212.2644, 2014.

[32] RZ Khasminskii. Principle of averaging for parabolic and elliptic differential equations and for markov processes with small diffusion. *Theory of Probability & Its Applications*, 8(1):1–21, 1963.

[33] Thomas G Kurtz. A limit theorem for perturbed operator semigroups with applications to random evolutions. *Journal of Functional Analysis*, 12(1):55–67, 1973.

[34] Grigorios A Pavliotis and Andrew M Stuart. *Multiscale methods: averaging and homogenization*, volume 53. Springer, 2008.

[35] G. L. Eyink and J. Xin. Self-similar decay in the kraichnan model of a passive scalar. *J. Stat. Phys.*, 100(3-4):679–741, 2000.

[36] M. Chaves, G. Eyink, U. Frisch, and M. Vergassola. Universal decay of scalar turbulence. *Phys. Rev. Lett.*, 86:2305–2308, 2001.

[37] A. Majda, I. Timofeyev, and E. Vanden-Eijnden. Stochastic models for selected slow variables in large deterministic systems. *Nonlinearity*, 19(4):769, 2006.

[38] F. Balboa Usabiaga, X. Xie, R. Delgado-Buscalioni, and A. Donev. The Stokes-Einstein Relation at Moderate Schmidt Number. *J. Chem. Phys.*, 139(21):214113, 2013.

[39] P. J. Atzberger. Stochastic Eulerian-Lagrangian Methods for Fluid-Structure Interactions with Thermal Fluctuations. *J. Comp. Phys.*, 230:2821–2837, 2011.

[40] A. Donev, A. L. Garcia, Anton de la Fuente, and J. B. Bell. Diffusive Transport by Thermal Velocity Fluctuations. *Phys. Rev. Lett.*, 106(20):204501, 2011.

[41] François Detcheverry and Lydéric Bocquet. Thermal fluctuations of hydrodynamic flows in nanochannels. *Physical Review E*, 88(1):012106, 2013.

[42] J. P. Hernandez-Ortiz, J. J. de Pablo, and M. D. Graham. Fast Computation of Many-Particle Hydrodynamic and Electrostatic Interactions in a Confined Geometry. *Phys. Rev. Lett.*, 98(14):140602, 2007.

[43] Tri T Pham, Ulf D Schiller, J Ravi Prakash, and Burkhard Dünweg. Implicit and explicit solvent models for the simulation of a single polymer chain in solution: Lattice boltzmann versus brownian dynamics. *J. Chem. Phys.*, 131:164114, 2009.

[44] P. J. Atzberger. A note on the correspondence of an immersed boundary method incorporating thermal fluctuations with Stokesian-Brownian dynamics. *Physica D: Nonlinear Phenomena*, 226(2):144–150, 2007.

[45] F. Balboa Usabiaga, R. Delgado-Buscalioni, B. E. Griffith, and A. Donev. Inertial Coupling Method for particles in an incompressible fluctuating fluid. *Comput. Methods Appl. Mech. Engrg.*, 269:139–172, 2014. Code available at https://code.google.com/p/fluam.

[46] M Rex and H Löwen. Dynamical density functional theory for colloidal dispersions including hydrodynamic interactions. *The European Physical Journal E*, 28(2):139–146, 2009.

[47] U. Frisch, A. Mazzino, A. Noullez, and M. Vergassola. Lagrangian method for multiple correlations in passive scalar advection. *Physics of Fluids*, 11(8):2178, August 1999.

[48] A. Sierou and J. F. Brady. Accelerated Stokesian Dynamics simulations. *J. Fluid Mech.*, 448:115–146, 2001.

[49] J Courtenay Lewis. On the einstein-stokes diffusion coefficient for brownian motion in two dimensions. *Physics Letters A*, 44(4):245–246, 1973.

[50] T. Keyes and Irwin Oppenheim. Bilinear hydrodynamics and the stokes-einstein law. *Phys. Rev. A*, 8:937–949, 1973.

[51] L. Greengard and J. Lee. Accelerating the nonuniform fast fourier transform. *SIAM Review*, 46(3):443–454, 2004.

[52] J. C Mattingly, T. Suidan, and E. Vanden-Eijnden. Simple systems with anomalous dissipation and energy cascade. *Communications in Mathematical Physics*, 276(1):189–220, 2007.

[53] T. Komorowski and S. Peszat. Transport of a passive tracer by an irregular velocity field. *J. Stat. Phys.*, 115(5-6):1361–1388, 2004.

[54] J. Bechhoefer, J.-C. Géminard, L. Bocquet, and P. Oswald. Experiments on tracer diffusion in thin free-standing liquid-crystal films. *Phys. Rev. Lett.*, 79:4922–4925, 1997.

[55] P. Español, J.G. Anero, and I. Zúñiga. Microscopic derivation of discrete hydrodynamics. *J. Chem. Phys.*, 131:244117, 2009.

[56] C Kipnis, S Olla, and SRS Varadhan. Hydrodynamics and large deviation for simple exclusion processes. *Communications on Pure and Applied Mathematics*, 42(2):115–137, 1989.

[57] Claude Kipnis and Stefano Olla. Large deviations from the hydrodynamical limit for a system of independent brownian particles. *Stochastics: An International Journal of Probability and Stochastic Processes*, 33(1-2):17–25, 1990.

[58] B. Schulz, D. Täuber, F. Friedriszik, H. Graaf, J. Schuster, and C. Von Borczyskowski. Optical detection of heterogeneous single molecule diffusion in thin liquid crystal films. *Physical Chemistry Chemical Physics*, 12(37):11555–11564, 2010.

[59] F. Croccolo, H. Bataller, and F. Scheffold. A light scattering study of non equilibrium fluctuations in liquid mixtures to measure the Soret and mass diffusion coefficient. *J. Chem. Phys.*, 137:234202, 2012.

[60] P. N. Segrè, R. W. Gammon, and J. V. Sengers. Light-scattering measurements of nonequilibrium fluctuations in a liquid mixture. *Phys. Rev. E*, 47:1026–1034, Feb 1993.

[61] A. Vailati and M. Giglio. Nonequilibrium fluctuations in time-dependent diffusion processes. *Phys. Rev. E*, 58(4):4361–4371, 1998.

[62] Eric Vanden-Eijnden. Numerical techniques for multi-scale dynamical systems with stochastic effects. *Communications in Mathematical Sciences*, 1(2):385–391, 2003.

[63] W. E, W. Ren, and E. Vanden-Eijnden. A general strategy for designing seamless multiscale methods. *J. Comp. Phys.*, 228(15):5437–5453, 2009.

[64] Thomas Schaffter. Numerical integration of sdes: a short tutorial. *Swiss Federal Institute of Technology in Lausanne (EPFL), Switzerland, Unpublished manuscript*, 2010.

[65] M. Cai, A. J. Nonaka, J. B. Bell, B. E. Griffith, and A. Donev. Efficient Variable-Coefficient Finite-Volume Stokes Solvers. Arxiv preprint 1308.4605, 2013.

[66] B.E. Griffith. An accurate and efficient method for the incompressible Navier-Stokes equations using the

projection method as a preconditioner. *J. Comp. Phys.*, 228(20):7565–7595, 2009.

[67] Sandra May, Andrew Nonaka, Ann Almgren, and John Bell. An unsplit, higher-order godunov method using quadratic reconstruction for advection in two dimensions. *Communications in Applied Mathematics and Computational Science*, 6(1):27–61, 2011.

[68] Andy Nonaka, S May, Ann S Almgren, and John B Bell. A three-dimensional, unsplit godunov method for scalar conservation laws. *SIAM Journal on Scientific Computing*, 33(4):2039–2062, 2011.

[69] A. Donev, E. Vanden-Eijnden, A. L. Garcia, and J. B. Bell. On the Accuracy of Explicit Finite-Volume Schemes for Fluctuating Hydrodynamics. *CAMCOS*, 5(2):149–197, 2010.

[70] S. Delong, F. Balboa Usabiaga, R. Delgado-Buscalioni, B. E. Griffith, and A. Donev. Brownian Dynamics without Green's Functions. Submitted to J. Chem. Phys., 2014.